Pergamon

Geochimica et Cosmochimica Acta, Vol. 60, No. 21, pp. 4037–4057, 1996
Copyright © 1996 Elsevier Science Ltd
Printed in the USA. All rights reserved
0016-7037/96 $15.00 + .00

PII S0016-7037(96)00231-1

# Porewater pH and authigenic phases formed in the uppermost sediments of the Santa Barbara Basin

CLARE E. REIMERS,[1] KATHLEEN C. RUTTENBERG,[2] DONALD E. CANFIELD,[3] MATTHEW B. CHRISTIANSEN,[4] and JONATHAN B. MARTIN[5]

[1]Institute of Marine and Coastal Sciences, Rutgers University, New Brunswick, NJ 08903-0231, USA
[2]Woods Hole Oceanographic Institution, Woods Hole, MA 02543, USA
[3]Max Planck Institute for Marine Microbiology, Fahrenheitstrasse 1, D-28359, Bremen, Germany
[4]Scripps Institution of Oceanography, La Jolla, CA 92093, USA
[5]Department of Geology, University of Florida, Gainesville, FL 32611-7340, USA

(*Received December* 22, 1995; *accepted in revised form June* 28, 1996)

**Abstract**—In this paper porewater and solid phase analyses are used in combination with in situ $O_2$ and pH microelectrode measurements to characterize early diagenetic processes in the uppermost sediments of the Santa Barbara Basin, California. Rapid reduction of dissolved oxygen, nitrate, solid phase manganese and iron, and dissolved sulfate is observed. Between sediment depths of 0 and 2 cm, reductive solubilization of ferric iron phases releases $Fe^{2+}$, adsorbed phosphate, and fluoride to the porewaters and contributes to a sharp increase in porewater pH. Between 2 and 4 cm, sulfate reduction rates peak, pH levels off, and acid volatile sulfides and pyrite become the dominant forms of solid phase iron. Saturation state calculations, which depend largely on pH, indicate that the porewaters of the Santa Barbara Basin become saturated with respect to carbonate fluorapatite and calcite within the first 0.25 mm of the sediment and are highly supersaturated by and below 2 cm. In spite of this result, porewater evidence of phosphate and fluoride removal into a solid phase is observed only in the first ~5 cm of some cores, whereas dissolved Ca profiles suggest dispersed calcite precipitation throughout the sediment column. This finding is interpreted as an indication of the nonsteady state nature of the surface reactions that may, given sufficient nucleation sites and time, lead to carbonate fluorapatite genesis in anoxic sediments.

Finally, microelectrode pH profiles from two other basins in the California Borderlands are presented. These demonstrate that the porewaters of the Santa Barbara Basin are more alkaline than those of other basins. This outcome is attributed to the lack of particle mixing and a unique interplay between Fe liberation and FeS precipitation reactions in the Santa Barbara Basin.

## 1. INTRODUCTION

Many of the active biogeochemical processes that bring about changes in sedimentary particles begin only after particles reach the sediment–water interface. During early diagenesis, solid-phase transformations occur together with the initial stages of sediment compaction and often through a rapid succession of redox and pH conditions. In the present study, our goal was to resolve the initial changes in redox chemistry and pH that might lead to or limit the precipitation of authigenic minerals such as carbonate fluorapatite, low-Mg calcite, and pyrite in the sediments of the Santa Barbara Basin.

The Santa Barbara Basin is a modern marine basin where the sediments are varved and organic-rich (Hülsemann and Emery, 1961; Soutar and Crill, 1977; Schimmelmann et al., 1990). Generally, carbonate fluorapatite, low-Mg calcite, and pyrite are characteristic of both modern and ancient organic-rich sediments. What is unclear is whether these minerals tend to precipitate together or only in an ordered sequence. Froelich et al. (1988), Glenn and Arthur (1988), and Glenn et al. (1988) argue for a carbonate fluorapatite-$CaCO_3$ diagenetic sequence constrained vertically by downward increasing porewater concentrations of carbonate alkalinity. Glenn and Arthur (1988) also suggest that depending on the availability of reactive iron, pyrite precipitation may be coincident with carbonate fluorapatite (CFA) precipitation, or it may continue after that of CFA. Departing from this viewpoint, Ruttenberg and Berner (1993) suggest diagenetic redistribution of organic P into CFA may be a nearly continuous process at least to 50 cm in terrigenous dominated coastal sediments. Their analysis implies that CFA formation is not restricted to very shallow burial depths and may occur concurrently with $CaCO_3$ precipitation.

We chose the Santa Barbara Basin as a place to study whether there is evidence for strict mineral paragenesis (i.e., a sequence of precipitation) in surface sediments because we were hopeful that progressive change could be followed by sampling the nonbioturbated, millimeter-scale layers in these sediments (Soutar and Crill, 1977; Schimmelmann et al., 1990). Another property of these sediments, their high porosity, meant that delicate microelectrodes could easily penetrate to depths of 5–10 cm without being broken. In situ microelectrode measurements became pivotal during the course of this study because they proved to be the only means to accurately determine porewater pH profiles. We describe how in situ pH profiles from the SBB reveal diagenetic processes, and we compare them to profiles from other benthic environments and to published model predictions for pH in anoxic porewaters.

## 2. SAMPLING AND EXPERIMENTAL METHODS

Our analysis focuses on collections within a 6 $km^2$ area located near the center of the Santa Barbara Basin (SBB) (Fig. 1). In this

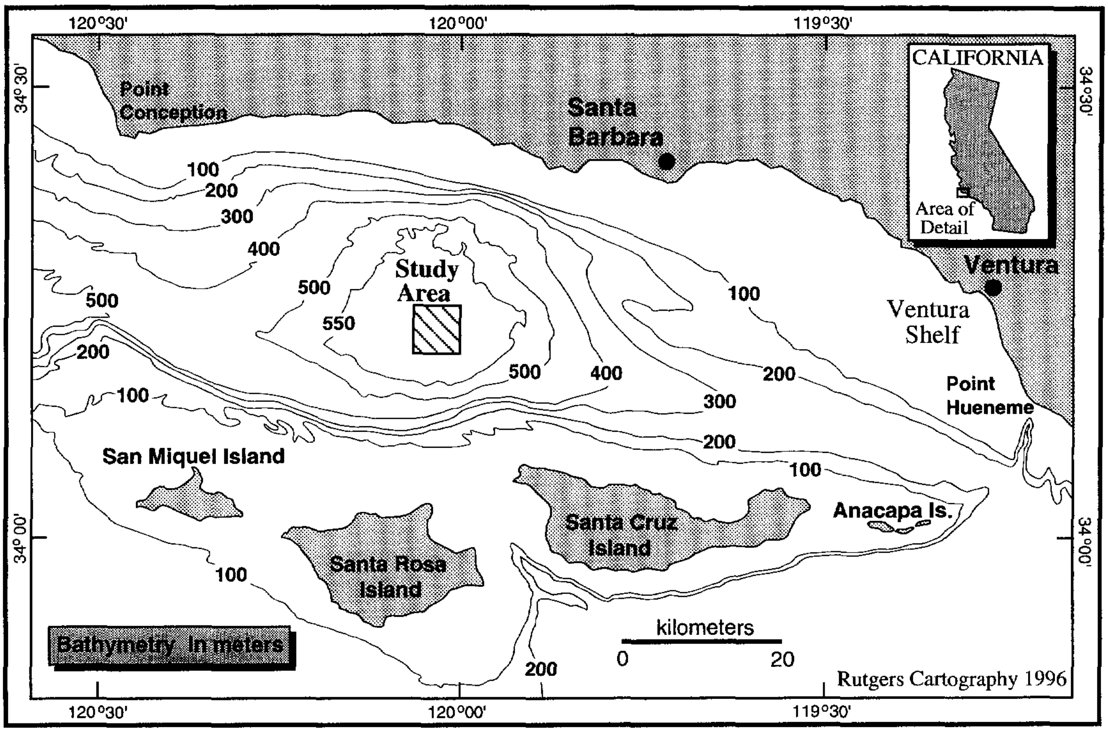


FIG. 1. Bathymetry of the Santa Barbara Basin. The rectangle encloses the sampling area.

area the water depth is 585 ± 5 m, and the sediments are well varved (Grant, 1991). Sediment cores and bottom water samples were collected during cruises in February, June, and October, 1988, June, 1989, June, 1991, and November, 1993. In addition, on three occasions we used an instrument tripod (or lander) equipped with a Photosea model 4000 Stereo camera and microprofiler instrument (Reimers, 1987; Reimers et al., 1992) to take color photographs of the seafloor in time-lapse and to measure with microelectrodes in situ resistivity, oxygen, and/or pH profiles in the uppermost sediments. A summary of the dates and locations of all field measurements and collections from which data are reported is presented in Table 1.

### 2.1. Microelectrode Measurements

Over-penetration of the profiler's tripod and imperfect microsensor operation hampered our initial efforts to measure resistivity, oxygen, and pH across the sediment-water interface in situ with microelectrodes, but we persisted in our attempts until complete profiles of all three parameters had been successfully measured.

During October 1988, the microprofiler was configured with six oxygen microelectrodes, one pH microelectrode, one resistivity electrode, and one Ag/AgCl reference electrode (used opposite both pH and $O_2$ sensors). By June 1991 the microprofiler was redesigned to operate up to 4 pH (or $pCO_2$) microelectrodes, 3 $O_2$, and 1 resistivity microelectrode with separate Ag/AgCl references for pH and $O_2$. Two deployments with full complements of sensors were attempted in 1991. Only pH and resistivity sensors were deployed in 1993. The designs of the sensors were as described by Cai and Reimers (1993), and the Ag/AgCl reference wires were surrounded by seawater saturated with AgCl and separated from the outside seawater by an agar plug. The resolution of the profiling was set at 1 mm vertical steps in 1988, but reduced to 0.25 mm steps over the upper portions of the profiles measured in 1991 and 1993.

Bottom water readings were used as reference points for calibration (Reimers, 1987; Cai and Reimers, 1993). If readings changed appreciably for a given microelectrode before and after profiling the sediments, the profile was rejected or is reported noting the direction of change. A change in the electrode response from before profiling to after can signal that the sensor's response has been affected either by damage and associated electrical leakage, or by chemical deposits on surfaces of the sensor or it's reference electrode.

Shipboard pH microelectrode measurements were made in 1993 by placing a subcore from a box core (see below) in a temperature controlled water bath (6°C). The microelectrode was introduced stepwise from above using a micromanipulator, and readings (in millivolts) were recorded from a pH meter.

### 2.2. Sediment Collection and Subsampling

The coring devices used were a Soutar box corer and a standard Kasten corer. The Kasten corer was used to obtain sediments from below the zone of earliest diagenesis. It was fitted with a 20 × 20 × 200 cm stainless steel barrel and clearly over-penetrated the seafloor, so that the first 30–40 centimeters of the sediment column were not recovered with these cores. The 30 × 30 × 100 cm aluminum box of the Soutar corer has stops to prevent over-penetration and a tightly sealing lid to minimize water exchange and disturbance of the sediment–water interface during core retrieval. With it, the upper 75–85 centimeters of sediment were consistently retrieved. A Niskin bottle, clamped to the outer frame of the box corer, collected bottom water samples from ca. 0.5 m above the seafloor when the spades of the box corer closed.

Subsampling of the Kasten cores was done on the ship's deck after lying the corer horizontal and removing one half of the four-sided barrel. Approximately 3 cm of the exposed sediment on the open face of the core was scraped off with a spatula, and then at measured distances down core, cylindrical plugs of sediment were drawn into plastic 60 mL syringes that had been opened and beveled off at the needle end. The modified syringes were inserted parallel to the bedding so that each sampled a layer of sediment that was approximately 3 cm thick. This subsampling was done quickly to minimize warming and air exposure, and then the syringes plus sediment were removed to a refrigerated laboratory van (6 ± 3°C) and placed inside a $N_2$-filled glove bag.

Table 1. Summary of Collections and Reported Geochemical Analyses

| Collection[1] | Date (M-D-Y) | Latitude °N | Longitude °W | Analyses[2] |
|---|---|---|---|---|
| K3 | 2-23-88 | 34 13.93 | 120 02.07 | pw |
| BC8 | 2-23-88 | 34 13.95 | 120 02.40 | pw, ATP |
| BC12 | 2-24-88 | 34 13.52 | 120.01.22 | pw, ATP, CNP |
| BC21 | 2-25-88 | 34 13.79 | 120 01.48 | pw, ATP, CNP, XRD, ICP |
| K22 | 2-25-88 | 34 13.87 | 120.01.00 | pw |
| BC54 | 6-21-88 | 34 14.59 | 120 02.36 | pw, ATP, NAA |
| BC58 | 6-22-88 | 34 14.02 | 120 02.37 | pw, $SO_4$rr, S, Fe |
| BC61 | 6-22-88 | 34 14.04 | 120 02.42 | pw, ATP |
| BC68 | 6-24-88 | 34 13.82 | 120 02.51 | pw, ATP, CNP |
| BC78 | 10-5-88 | 34 13.83 | 120 02.17 | pw, ATP, CNP, Xradiog. |
| IMP81 | 10-6-88 | 34 13.76 | 120 01.74 | $O_2$, R, photos. |
| BC82 | 10-6-88 | 34 13.88 | 120 02.93 | pw, ATP, Xradiog. |
| BC100 | 7-3-89 | 34 13.7 | 120 02.4 | pw |
| BC109 | 6-7-91 | 34 14.1 | 120 02.1 | pw, Xradiog. |
| IMP110 | 6-7-91 | 34 13.85 | 120 01.9 | $O_2$, R, photos. |
| BC114 | 6-8-91 | 34 14.2 | 120 02.2 | pw, Xradiog. |
| BC118 | 6-9-91 | 34 13.7 | 120 01.7 | pw |
| IMP120 | 6-10-91 | 34 13.93 | 120 02.04 | $O_2$, R, photos. |
| IMP202 | 11-6-93 | 34 13.69 | 120 01.77 | R, pH |
| IMP203 | 11-7-93 | 34 13.81 | 120.01.80 | pH |
| BC204 | 11-8-93 | 34 13 .43 | 120 01.61 | pH |

[1] BC = box core, K = Kasten core, IMP = in situ microprofiler
[2] pw = pore water chemical analyses (refer to Appendix 1), ATP = adenosine triphosphate (reported in Reimers et al., 1990), CNP = % carbon, nitrogen, phosphorus in solids, $SO_4$rr. = sulfate reduction rate, S = % solid phase sulfur, acid volatile sulfur, and pyrite sulfur, Fe = % solid phase iron, XRD = X-ray diffraction mineralogy, ICP = inductively coupled plasma elemental analyses, NAA = neutron activation analysis, Xradiog. = X-radiograph, pH = pH microelectrode profiling, $O_2$ = oxygen microelectrode profiling, R = resistivity electrode profiling, photos = bottom photographs.

The box cores were subsampled with multiple subcores made from sections of 7.5 cm diameter butyrate tubing and in October 1988 and June 1991 with X-radiograph slabs. These tubes and slabs were pushed in by hand, capped on top and bottom, and then removed to the refrigerated van. Overlying water, which was 10–25 cm deep in the box, was not drained from the cores before subcoring, but the cores were inspected to make sure the surface, which is characteristically covered with a *Beggiatoa* mat (Soutar and Crill, 1977), was intact.

At least one subcore removed from each box core was designated for immediate vertical sectioning and porewater extraction. During the 1988 cruises, another was also sectioned for ATP extraction (Reimers et al., 1990). Sectioning was implemented with an extrusion device described by Shaw (1989). In a $N_2$-filled glove bag, in the cold van, overlying water was collected from above the sediment, then cylindrical slices of sediment (0.25, 0.5, or 1 cm thick) were extruded from the subcore tubes into a matching acrylic funnel, and the funnel was inverted to transfer the sample intervals into acid-cleaned, Nalgene, polyethylene, 50 $cm^3$, centrifuge tubes.

After a porewater subcore was entirely sectioned, the centrifuge tubes were capped inside the glove bag, removed, centrifuged, and transferred into a clean $N_2$-filled glove bag where the supernatant waters were removed, filtered, and divided into volumes that were either acidified or left nonacidified. Both the centrifuge (Sorvall SS-3) and the filtering glove bag were set up in the cold van so that the samples were kept at in situ temperatures until the porewaters were separated from the solids. Porewaters were extracted from the Kasten core by the same techniques except that the centrifuge tubes were filled with mud transferred to the loading funnel from the syringe samplers.

### 2.3. Chemical Analyses of Dissolved Constituents

Porewater samples were analyzed for as many as twelve dissolved constituents or parameters using techniques described briefly in Appendix A. Sulfide sample splits were taken and fixed with reagents within the glove bag, immediately after filtering, or when the HPLC method of Vetter et al. (1989) was used, before filtering. Prior to all other analysis, the filtered water samples were stored in clear, polystyrene, 5 $cm^3$ tubes with polypropylene snap caps. A 0.02 $cm^3$ aliquot of ultraclean 6 N HCl was added to each of the 5 $cm^3$ fractions that were designated acidified. Analyses of dissolved inorganic phosphate ($\Sigma PO_4$), $Fe^{2+}$, $Mn^{2+}$, and $NO_3^-$ + $NO_2^-$ utilized water samples that were acidified. All other analyses were performed on nonacidified samples with the exception of some of the $Ca^{2+}$ measurements which were determined using previously titrated alkalinity samples. All $\Sigma PO_4$, $\Sigma H_2S$, $\Sigma NH_4$, and $Mn^{2+}$ analyses were performed (or in the case of $\Sigma H_2S$ by HPLC, initiated) at sea within 24 h of sample collection. $Fe^{2+}$, $F^-$ (except BC 100), and total alkalinity were determined within one week of sample collection either at sea or in the laboratory. Most of the $\Sigma I$, $Ca^{2+}$, $Mg^{2-}$ concentrations, and the $SO_4^{2-}$ concentrations that were determined by $BaSO_4$ turbidity, were measured within 2 months of collection. Fluoride within samples of BC100 and other $\Sigma I$, $Ca^{2+}$, $Mg^2$, and $SO_4^{2-}$ determinations, from samples that had been stored longer than two months, were corrected for evaporation artifacts by dividing the

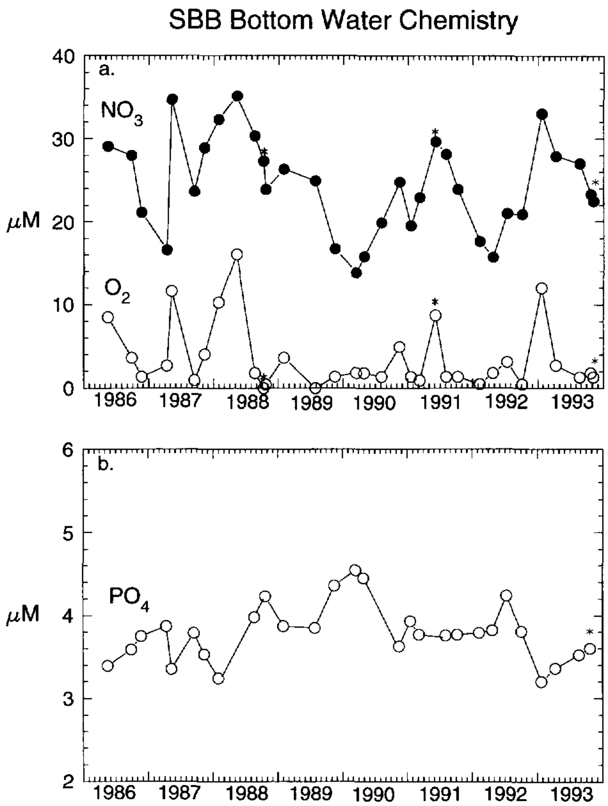


FIG. 2. Variations in bottom water chemistry of the Santa Barbara Basin. Except for three sets of values (marked with stars) determined during cruises in this study, these data are from CalCOFI program data reports (Scripps Institution of Oceanography 1986–1993). They represent analyses of water samples collected by Niskin bottle from $<1$–25 meters above bottom. The phosphate concentration of the sample collected on 5 Aug. 1990 is not plotted. It was determined to be $>4.1$ $\mu$M, the maximum full-scale setting of the auto-analyzer for that cruise (A. Mantyla, pers. commun., 1990).

measured values by the ratio of the $Cl^-$ concentration of the sample to bottom water $Cl^-$ (547.6 mM). The Cl concentrations of these partially evaporated samples were determined by $AgNO_3$ titration (Gieskes and Peretsman, 1986) (average s.d. $\times$ 2 = 0.8%) or were measured together with $SO_4^{2-}$ on a Dionex Series 4000I ion chromatograph equipped with an AS5A-5$\mu$ anion separator column and an anion micromembrane suppressor. IAPSO seawater was the standard for all ion chromatograph analyses. Spreadsheets of all of the porewater data and concentrations of bottom waters that were analyzed in tandem with the porewater samples may be obtained from C. Reimers. A specific set of bottom water samples were taken during 1993 by hydrocast and with a Niskin bottle on the microprofiler tripod. These samples were analyzed for dissolved oxygen using a high precision automated Winkler titration and reagents purged with $N_2$ (precision $\pm$ 0.5 $\mu$mol/kg), for total-$CO_2$ with a SOMMA/coulometer ($\pm 2$ $\mu$mol/kg) (Johnson et al., 1985, 1987), for total alkalinity by automated closed cell titration at 25°C ($\pm 3$ $\mu$mol/kg) (Bradshaw and Brewer, 1988), and for nitrate, silicate, and phosphate using a LACHAT Quikchem AE flow injection autoanalyzer.

### 2.4. Sulfate Reduction Rate Determinations

Sulfate reduction rates were determined in a subcore of one box core (BC58; Table 1). The subcore was collected at sea, sealed, stored in the shipboard refrigerated van, and returned to a shore-based refrigerated laboratory for incubations at the in situ temperature using radiolabelled $^{35}SO_4$ by the core injection technique of Jørgensen (1978) and Westrich (1983). Incubations were initiated 2 days after the core was collected and terminated 24 h later by freezing. Radiolabelled sulfides were collected by cold acid distillation of 2 cm sections of the frozen sediment subcore in a 10% $SnCl_2$/6 N HCl solution (Canfield, 1989).

### 2.5. Solid Phase Analyses

Solid phase chemical distributions were determined on selected box cores. Sediment solids remaining after the porewaters were removed by centrifugation (BC68 and BC78) or collected from a separate box core subcore (BC 21) were analyzed for carbon, nitrogen, and phosphorus. These samples were first freeze-dried, ground with an agate mortar and pestle, homogenized, redried in an oven at 100°C, and then stored in a desiccator. The solids from BC21 were the only samples that prior to freezing were exposed to an $O_2$-containing atmosphere. This subcore was sampled in our shore-based laboratory by layers defined by color changes in the sediment rather than by extruded thicknesses. The volume of each layer, carefully scraped off the surface of the subcore, was used to estimate the layer thickness within the core tube (Schmidt and Reimers, 1991). Total carbon and nitrogen were determined with a Perkin-Elmer model 2400 CHN elemental analyzer. Inorganic-C was determined by coulometric titration after $CO_2$ liberation with 1 N HCl using a Coulometrics Carbon analyzer. Organic carbon was estimated as the difference between total and carbonate-C. Solid phase phosphorus was partitioned by extracting untreated and ashed (500°C, 2 h) samples with 1 N HCl and then determining the phosphate concentration within aliquots of supernatant removed after centrifugation, by molydate-blue spectrophotometry (Froelich et al., 1988; Aspila et al., 1976). Total phosphorus contents correspond to determinations from the ashed sample. Inorganic phosphorus was estimated from the phosphate extracted from the untreated sample, and organic phosphorus was defined as the difference between total and inorganic determinations. These methodological definitions do not clearly separate apatitic from plankton or microbially derived phosphorus (Ruttenberg, 1992). The inorganic fraction may include phosphate that is sorbed onto solid phases such as iron oxyhydroxides, or forms of biologically produced phosphate such as intercellular poly-phosphate inclusions.

All C, N, and P concentrations reported were calculated on a salt-free sediment basis. The salt contents of the solid samples were estimated from triplicate determinations of chlorinity in water aliquots that had been mixed with weighed splits of dried sediment.

Using a multiple-extraction scheme described by Canfield (1988, 1989), solid phase iron was partitioned between reactive (dominantly ferrihydrite and lepidocrocite), crystalline (hematite and goethite), monosulfide-Fe, and pyrite-Fe fractions in samples from the one box core analyzed for sulfate reduction rate (BC 58). Total iron concentrations were also determined for us in samples of BCs 54 and 21, by colleagues from Woods Hole Oceanographic Institution and the US Geological Survey, Denver office, using neutron activation analysis (NAA) and X-ray fluorescence (XRF) methods. The NAA also yielded estimates of %Al, %Mn, and rare earth element concentrations that have been reported by Olmez et al. (1991). The XRF analyses yielded percentages of Si, Al, Mg, Ca, Na, K, Ti, P, and Mn (J. Herring, USGS, pers. commun., 1988). These data may be requested from C. Reimers.

## 3. RESULTS

### 3.1. Bottom Water Cycles in the Santa Barbara Basin

This study involved repetitive sampling of the seafloor of the Santa Barbara Basin on timescales of months to years. On these timescales, many of the porewater and solid-phase characteristics of the sediments near the water-interface are moderately variable. Part of this variability is driven by changes in the rain rate of particulate material, and part is coupled to variations in bottom water chemistry. Fluctuating

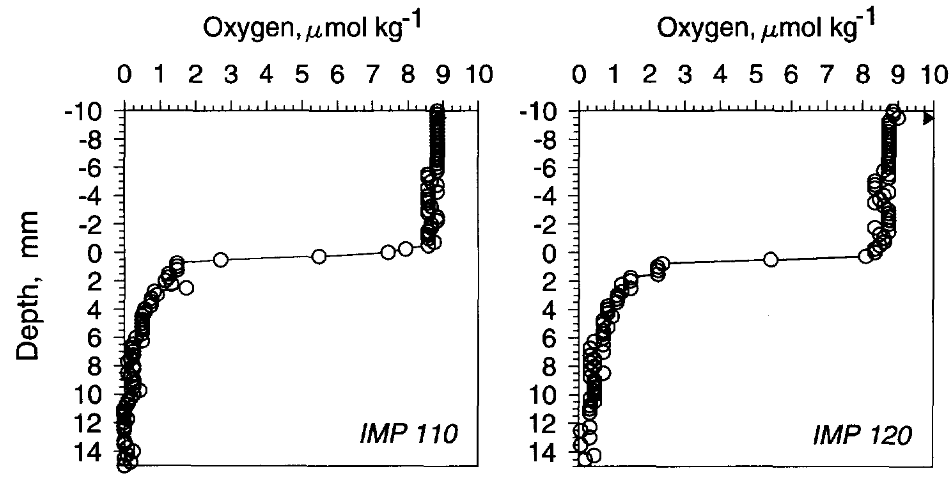


FIG. 3. Two examples of oxygen profiles measured across the sediment–water interface of the Santa Barbara Basin in June 1991. Solid triangles correspond to readings after the microelectrodes were retracted from the sediments.

conditions in the bottom water of the Santa Barbara Basin (Fig. 2) are manifestations of circulation and climatic events outside of the basin. The semiannual variability of the subsurface flow off Point Conception and within the California Bight (Lynn and Simpson, 1987) leads to the intrusion of colder denser, more oxygenated, and $NO_3^-$-rich water into the lower basin from sill depth, most commonly early in the year (Reimers et al., 1990). Figure 2 suggests that at certain times, such as in 1989 and 1990 (California drought years), climatic changes cause basin flushing to be relatively weak. These conditions lead to prolonged and greater reduction of $NO_3^-$ and $O_2$ levels, and to the elevation of phosphate that is released from the seabed. In Reimers et al. (1990), we documented that changes in bacterial biomass, and chemical and physical properties occur at the sediment–water interface (0–0.5 cm) between periods of high and low bottom water oxygen. The rapid evolution of sediment chemistry, with progressive burial below the sediment–water interface, is the focus of this paper.

### 3.2. Indicators of Overlapping Oxic, Suboxic, and Anoxic Diagenetic Reactions

Work by Sholkovitz (1973) demonstrates that interstitial water concentrations of total alkalinity, sulfate, ammonia, and phosphate measured to 130 cm depth in the Santa Barbara Basin can be predicted with a model of organic matter decomposition by sulfate reduction and authigenic precipitation of $CaCO_3$. However, this analysis does not consider dissolved and solid phase samples taken in fine-scale near the sediment–water interface. Photographs were taken of the sediment–water interface at the same times as the first two starred oxygen data points in Fig. 2; i.e., at periods of low and elevated bottom water oxygen. The color of the seafloor, the continuity of bacterial mat cover, and the presence or absence of mobile gastropods differed between these two time periods. In October 1988, the bottom photos revealed a continuous grey bacterial mat, and six oxygen microelectrodes deployed during IMP81 confirmed that the basin was completely anoxic by showing no change in response (recorded digitally as counts) during the course of their travel from positions roughly 5 cm above the sediment to depths of roughly 7 cm into the sediment. When tested after the cruise at 4°C in a cold-room, the response sensitivities of these same oxygen microelectrodes were approximately 0.5 $\mu$M $O_2$/count.

In contrast to the October 1988 results, the microprofiler and camera system deployed in situ in the basin in June 1991 detected a decrease in oxygen across a reddish-brown sediment–water interface (Fig. 3). Calibrated against bottom water oxygen concentrations determined by Winkler titrations of Niskin bottle samples, these profiles indicate that low levels of oxygen penetrated at least 4 mm into the sediment column. Levels $< 1$ $\mu$mol kg$^{-1}$ at depths of 4–10 mm are at the limit of detection and may not be significantly different from zero, since small shifts in the sensors' background currents could lead to signals in this range.

Nitrate + nitrite, Fe, and Mn porewater data determined from box core samples at different times in the central basin (Fig. 4, left panels) indicate that suboxic diagenetic reactions occur regularly in the uppermost sediments of the Santa Barbara Basin whether bottom water $O_2$ is present or not. Usually, nitrate, $Mn^{2+}$, and $Fe^{2+}$ are present together in the uppermost 3 cm, with dissolved iron enrichments extending to greater depths. In June 1991, when a relatively high bottom water $O_2$ concentration was measured, there was a large surface (0–0.25 cm) maximum in nitrate and nitrite in BC118, the only core of that cruise analyzed for nitrate and nitrite. High surface peaks of nitrate and nitrite were also measured in BCs 8, 21, and 78 indicating this feature can occur during high and low periods of the basin's bottom water $O_2$ cycle. Similar nitrate and nitrite peaks appear in porewater profiles reported by Froelich et al. (1988) from muds with *Thioploca spp.* mats that were collected beneath the oxygen minimum zone on the Peru margin. Such peaks may be an artifact of the centrifugation process, caused by the release of nitrate, stored within intercellular vacuoles of *Beggiatoa* for use in respiration (D. Nelson, pers. commun.; Fossing et al., 1995). We have estimated that there is never enough $O_2$ within the Santa Barbara Basin's bottom water for

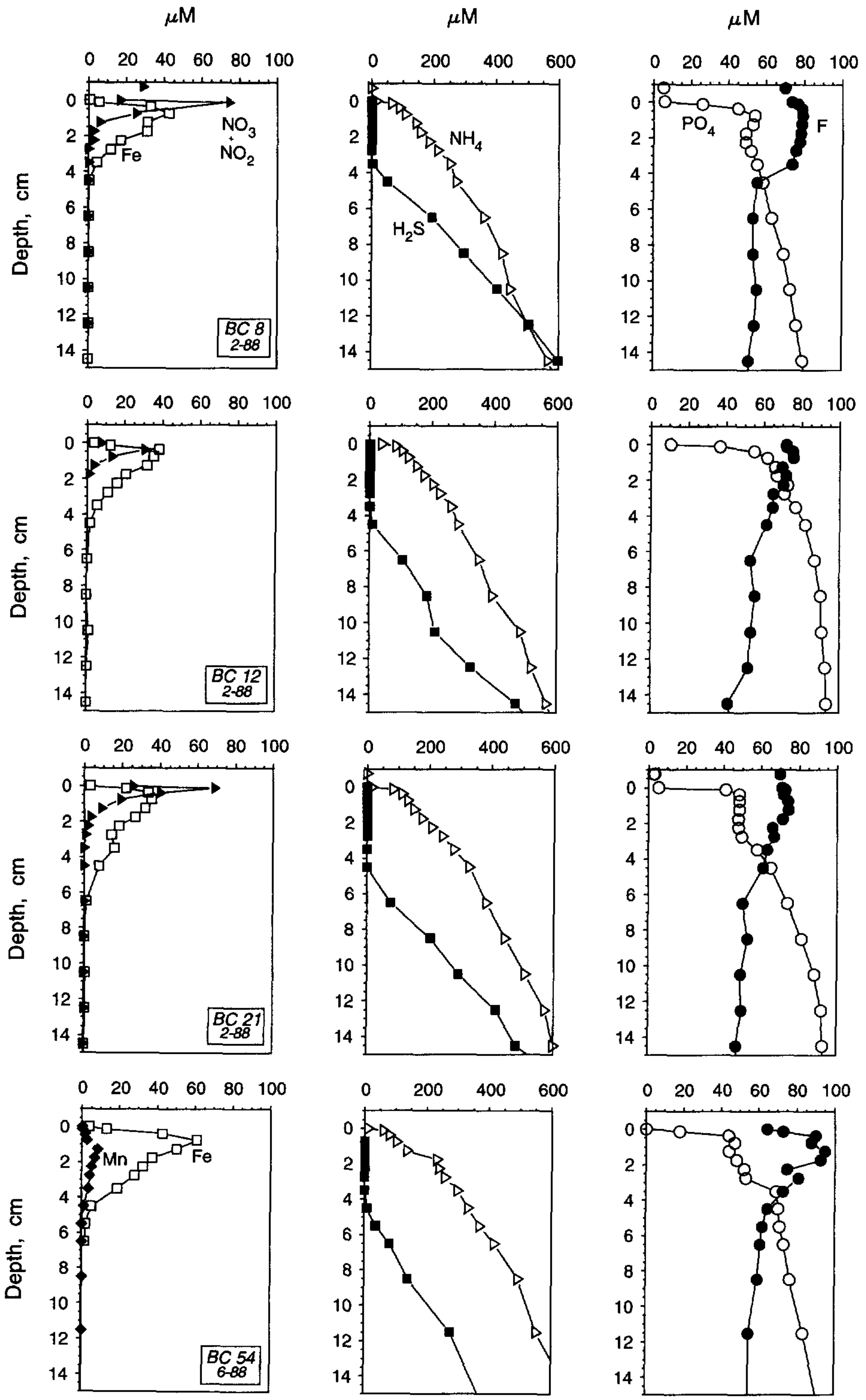


FIG. 4. Porewater profiles in the upper part of the sediment column of Santa Barbara Basin. Data points at −0.75 cm and 0 cm represent analyses of bottom waters and waters overlying the box core subcore, respectively. All other points represent porewaters separated by centrifugation. Symbols are used consistently throughout to identify the dissolved constituents nitrate + nitrite (▶), Mn (◆), Fe (□), total ammonia (▷), total sulfide (■), total phosphate (○) and fluoride (●).

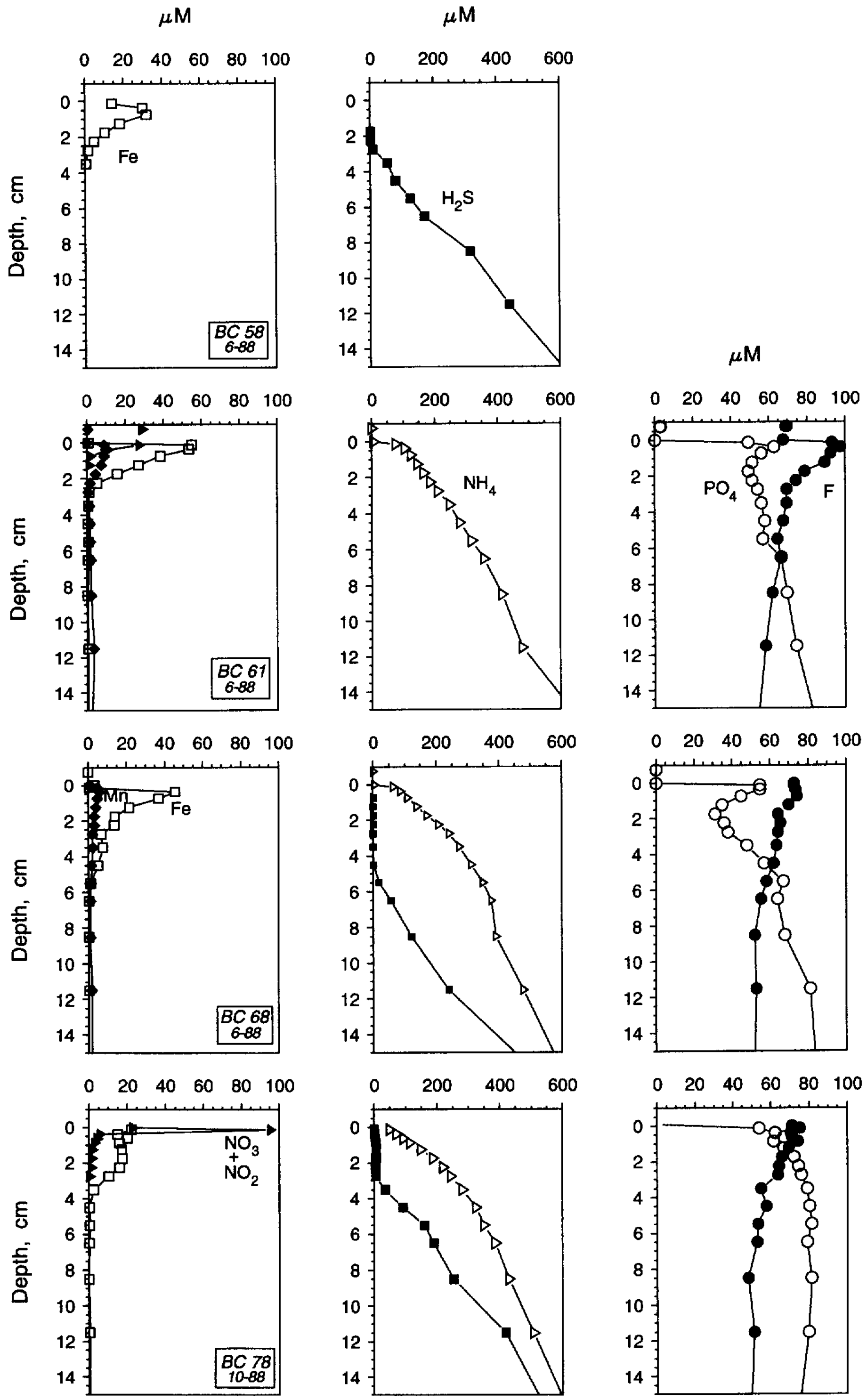


FIG. 4. (Continued)

molecular diffusion to support a nitrification rate high enough to maintain a nitrate gradient of 70–100 $\mu$M over 0.25 cm (we'd expect $\Delta O_2/\Delta NO_3 \sim 2D_{NO_3}/D_{O_2}$; if $NH_3 + 2O_2 \rightarrow HNO_3 + H_2O$).

Figure 4 also displays how profiles of dissolved nitrate and nitrite, Mn, and Fe relate to distributions of ammonia, sulfide, phosphate, and fluoride. Generally, sulfide is undetectable in the uppermost 2–4 cm of sediment (detection limit 0.5 $\mu$M), and sulfide concentrations do not begin to increase rapidly until depths where dissolved Fe is absent

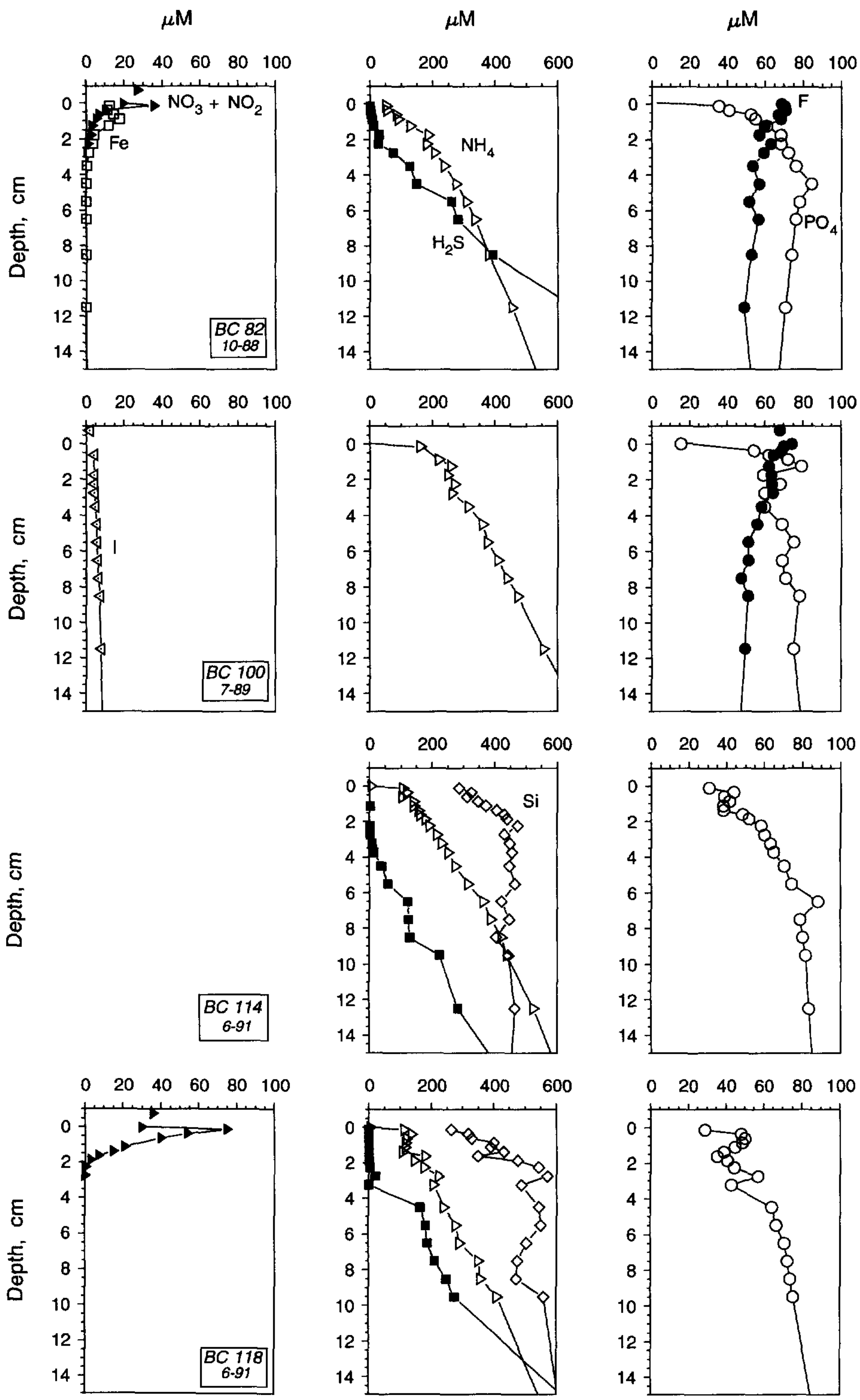


FIG. 4. (Continued)

(Reimers et al., 1990). Porewater sulfide concentrations are below detection in spite of the presence of high rates of sulfate reduction in the first 0–2, and 2–4 cm of sediment (Fig. 5). In this zone, Fe is clearly being reduced and reacting with sulfide (primarily in the 2–4 cm interval) to form iron sulfides represented as acid-volatile S and pyrite (Fig. 6) (Canfield and Raiswell, 1991). In the 0–2 cm zone, fluoride profiles tend to exhibit maxima that are greater than bottom water, and phosphate concentrations abruptly increase to 50–70 $\mu$M. Between approximately 0.5 and 3 cm

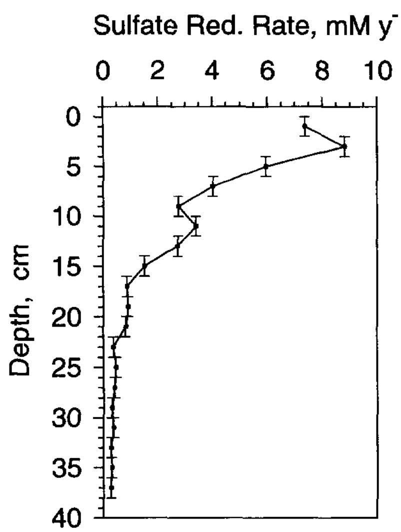


FIG. 5. A depth profile of sulfate reduction rate determined in BC 58 collected in June 1988.

depth, many phosphate profiles display minima. These minima vary in their definition. Phosphate profiles from BC 78 and BC 82 do not display minima. Collected in October 1988 when the basin's waters were anoxic (Fig. 2), these cores also had low but detectable concentrations of sulfide in the uppermost centimeters of sediment, and lower concentrations of $Fe^{2+}$ and $F^-$ (Fig. 4).

Extensions of the interfacial profiles of $\Sigma PO_4$, $F^-$, $\Sigma H_2S$, and $\Sigma NH_4$ can be seen in the Kasten core data (Fig. 7). These cores were missing the first 30–40 cm of sediment that was sampled by the box cores, but Fig. 7 demonstrates that throughout nearly 2 m of anoxic sediment, fluoride concentrations are essentially constant, while phosphate and ammonia are continuously accumulating in the porewaters. In fact, both box core and Kasten core data indicate that ammonia and phosphate are regenerated in a constant ratio of approximately 24.5:1 at all depths except in the uppermost few centimeters where an initial phosphate enrichment of roughly 60 $\mu$M is established (Fig. 8). BCs 78 and 82 (only 78 is shown in Fig. 8) are the only two cores that deviate from this pattern, but we have no definite explanation for why this is so. Possibly, since these two cores were analyzed on the same cruise with the same reagents, an analytical problem caused phosphate to be underestimated in deeper sections.

### 3.3. Alkalinity and pH Distributions

The only measure of the carbon dioxide system in porewater that was determined at different times in the basin was total alkalinity (TA). These profiles were all essentially the same (Fig. 9, upper left) and show the expected steady increase that is associated with pore solutions where sulfate reduction is the main mechanism for organic matter oxidation.

During our work in 1993, we measured pH profiles successfully with microelectrodes: in situ to better constrain the predictions of other carbonate system parameters, and in a core for comparison purposes. Figure 10 illustrates these pH microelectrode profiles. In situ readings of individual microelectrodes above the sediment–water interface were averaged, and this average equated to the bottom water pH (7.534) which was calculated (in the seawater scale) using constants and definitions compatible with UNESCO 1987 (also Dickson and Millero, 1987) from mean TA and $TCO_2$ measurements of 2347.2 $\mu$mol kg$^{-1}$ and 2345.0 $\mu$mol kg$^{-1}$, respectively (Table 2). The uncertainty in the bottom water pH introduced by the variability of the TA measurements is ±0.025 pH units. The microelectrode used on shipboard was calibrated with NBS standards after profiling, and a temperature correction (after Gieskes, 1969) was applied to the slope and the sensor's reading at pH 7, in order to assign pH values to the profile.

In situ pH is seen to generally increase with depth in these sediments, but a broad minimum centered at roughly 3 cm corresponds to the position where $NO_3^-$ and $NO_2^-$ concentrations approach zero (Fig. 4) and the zone of maximum sulfate reduction (Fig. 5).

Assuming pH values calibrated against NBS aqueous buffers can be equated to $pH_{SWS}$ by adding 0.08 to 0.18 (Hansson, 1973), the shipboard profile was generally shifted to a lower pH and showed a smaller magnitude increase with depth over the first 2–3 cm of sediment. The direction of these shifts are consistent with the pressure effect on equilibrium constants of the carbonate system, and generally illustrates the problems inherent in pH measurements made in decompressed cores (see Cai, 1992, chapter IV, for greater discussion).

### 3.4. Formation Factor Profiles and Accumulation Rates in the Basin

Formation factor profiles were computed from the relationship

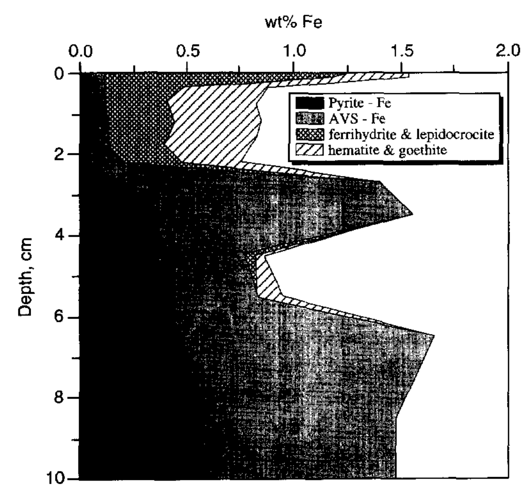


FIG. 6. The partitioning of Fe between extractable oxyhydroxide and sulfidic phases. Total Fe concentrations in Santa Barbara Basin sediments have been determined to be 3.3 ± 0.13 (unlisted NAA and XRF data (see methods); and Schmidt and Reimers, 1991) suggesting clay minerals are also an important source of solid phase Fe.

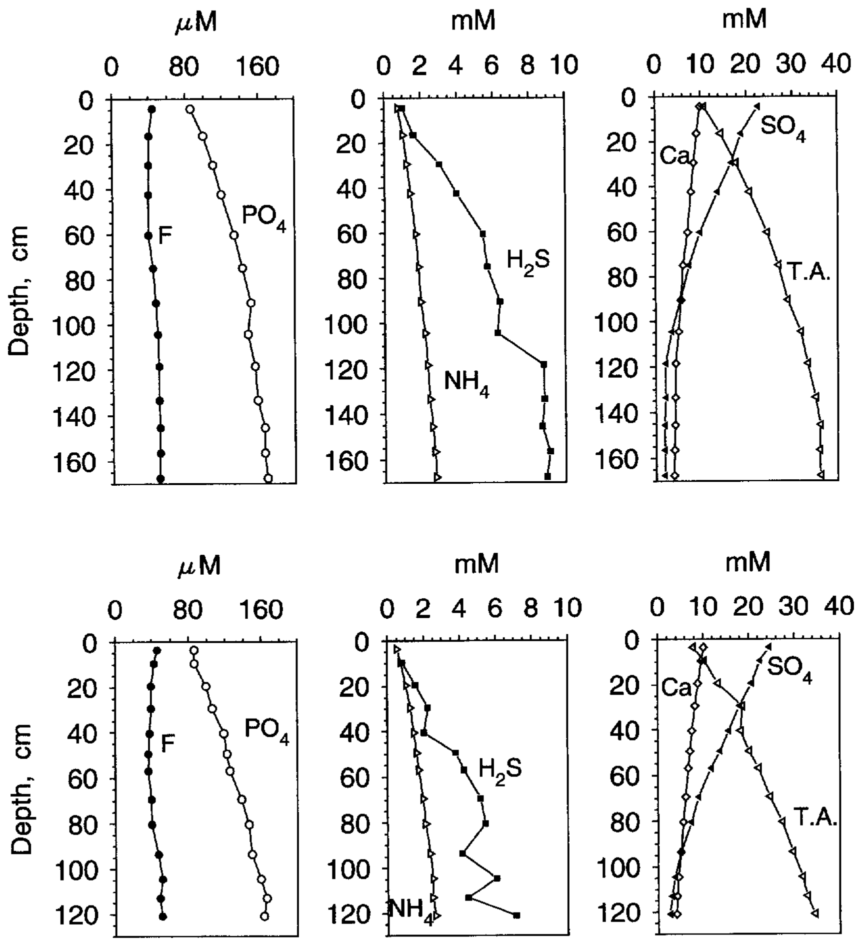


FIG. 7. Porewater constituent profiles from Kasten cores 3 (top) and 22 (bottom). The tops (zero depths) of these cores correspond to depths 30–40 cm below the sediment–water interface.

$$F = R_s/R_w,$$

where $R_s$ represents resistivity values measured by electrode in the sediment in situ, and $R_w$ represents the resistivity of the porewater which is assumed to equal an average of readings from the overlying bottom water (Fig. 11). In each profile, layering is evident, but specific laminae are difficult to identify. One exception is a layer of relatively high formation factor which marks flood-derived sediments that were deposited during 1982–1983 when an El Niño event caused high rates of rainfall and runoff, followed by enhanced terrigenous sedimentation off Southern California (Schimmelmann et al., 1990; Schmidt and Reimers, 1991). During October 1988, this layer was centered at 4.5 cm depth. The change in the depth position of this layer between October 1988 and June 1991 indicates a sedimentation rate of 4.2 $\pm$ 0.4 mm $y^{-1}$, essentially equal to $^{210}Pb$ and stratigraphic estimations of 3.9 and 4.0 mm $y^{-1}$ determined for deposits studied twenty years earlier (Koide et al., 1972). The rate derived from the resistivity measurements may be assumed to be highly accurate for the high porosity surface sediments, since the depth scales of the in situ profiles are unaffected by sampling disturbance. Furthermore, the low formation factor values in Fig. 11 indicate that to at least 10 cm depth, these muds have diffusivities that are 70–90% of those of seawater.

### 3.5. Solid Phase C, N, and P

Figure 12 illustrates depth profiles of organic and inorganic forms of carbon and phosphorus, and profiles of total nitrogen. The 1982–1983 El Niño layer is associated with near-surface minima in both the organic carbon and carbonate carbon concentration profiles, however, the inorganic C minimum precedes the organic C minimum. Surface (0–0.25 cm) organic C, N, and P enrichments reflect the development of the bacterial mat (Reimers et al., 1990). Below the surface there are no phorphorus-rich layers that would indicate the concentration of authigenic phosphate minerals. Ratios of organic C:total N:organic P approach the Redfield ratios of 106:16:1 in the surface mat but then scatter about an increasing trend with depth (Fig. 13). At and below 25 cm, the mean total N/organic P ratio of the solids is similar to the porewater regeneration ratio of 24.5:1 (Fig. 8). As was discussed by Sholkovitz (1973), such solid phase ratios are sensitive to analytical errors in the organic P content,

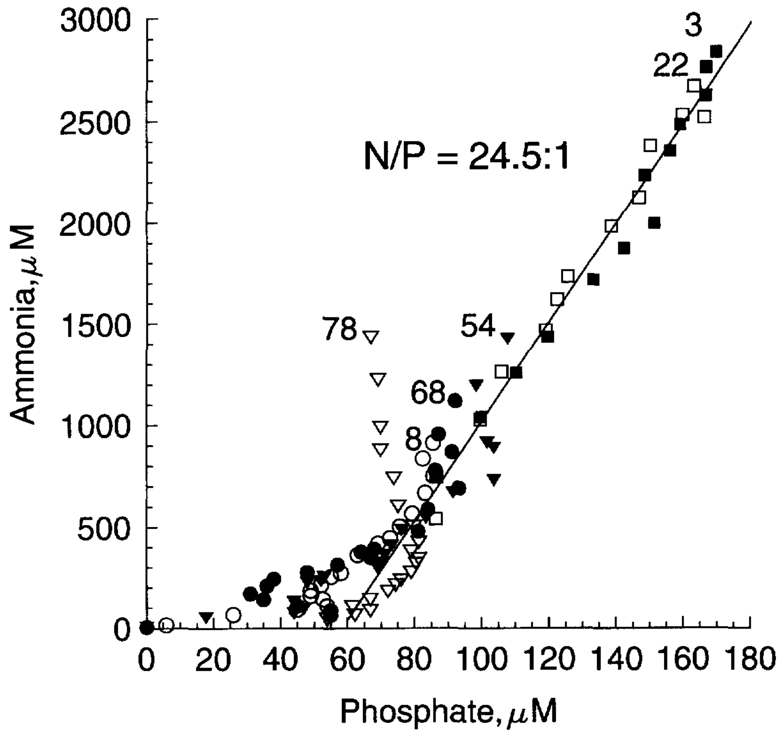


FIG. 8. Porewater phosphate vs. ammonia in the Santa Barbara Basin. Data from four box cores and two Kasten cores are shown, and the core numbers are given next to the deepest sample from each core. Regression of the Kasten core data suggests that ammonia and phosphate are regenerated at a ratio of 24.5:1. This regression relationship can be extended into the box core data as well.

which is assessed by subtracting two numbers of similar magnitude (total-inorganic P). However, overall trends demonstrate that relative to organic C, N and organic P are preferentially regenerated. The diagenetic regeneration of organic P has been suggested to lead to a steady down-core formation of authigenic carbonate fluorapatite in normal terrigenous-dominated sediments (Ruttenberg and Berner, 1993). The extent to which Santa Barbara Basin sediments may conform to this model or one of a depth-stratified sequence of authigenic mineral paragenesis is analyzed in the following sections.

## 4. DISCUSSION

### 4.1. CFA and Calcite Saturation Patterns

The first indicators of authigenic mineral formation we will examine involve equilibrium and saturation calculations for the uppermost Santa Barbara Basin sediments. The bottom waters of the Santa Barbara Basin have a low pH (7.534 ± .025 SWS) and appear undersaturated with respect to calcite ($\Omega = 0.90 \pm 0.05$) and CFA ($\log(\mathrm{IAP}/K_{sp}) = -.78$) largely because of the oxidation of organic matter that has led to the basin's oxygen depleted condition. In Fig. 14, profiles of carbonate ion concentration and calcite and CFA saturation states are extended into the sediments. Calcite saturation state was calculated based on the relationship

$$\Omega = [Ca^{2+}][CO_3^{2-}]/K_{sp}(\mathrm{calc}),$$

where the solubility product for calcite $K_{sp}(\mathrm{calc})$ is taken from Mucci (1983) and pressure corrected according to formulations in Millero (1979) ($K_{sp}(\mathrm{calc}) = 4.94 \times 10^{-7}$). The bottom water carbonate ion concentration was calculated with an iterative routine from the data in Table 2 and carbonate equilibrium relationships (Park, 1969), using equilibrium constants calculated for in situ temperature, salinity, and pressure from relationships in UNESCO, 1987. Bottom water $[Ca^{2+}]$ was estimated from salinity to equal 10.056 mmol kg$^{-1}$.

CFA saturation state was calculated in the same manner presented by Jahnke et al. (1983) and Ruttenberg and Berner (1993) whereby the ion activity product (IAP) for apatite, of the stoichiometry $Ca_{9.54}Na_{0.33}Mg_{0.13}(PO_4)_{4.8}(CO_3)_{1.2}(F)_{2.48}$, was ratioed to a solubility product that was itself dependent on the carbonate ion activity. Total ion activity coefficients were estimated to be approximately equal to values listed for seawater by Millero and Schreiber (1982). Given the presence of $HS^-$, DOC, high solid to solution ratios and a need for temperature and pressure corrections, these activity coefficients should be viewed as questionable but the best one can do given available ion pairing models.

Two other steps taken to generate Fig. 14 were porewater pH was set by selecting the best in situ pH profile in terms of electrode stability and reproducibility (Fig. 10b, profile plotted with triangles), then simple curves were fit to compilations of all TA, total-phosphate, ammonia, silica, sulfide, Ca, Mg, and fluoride profiles to approximate the concentrations of these species with single depth functions.

We assumed

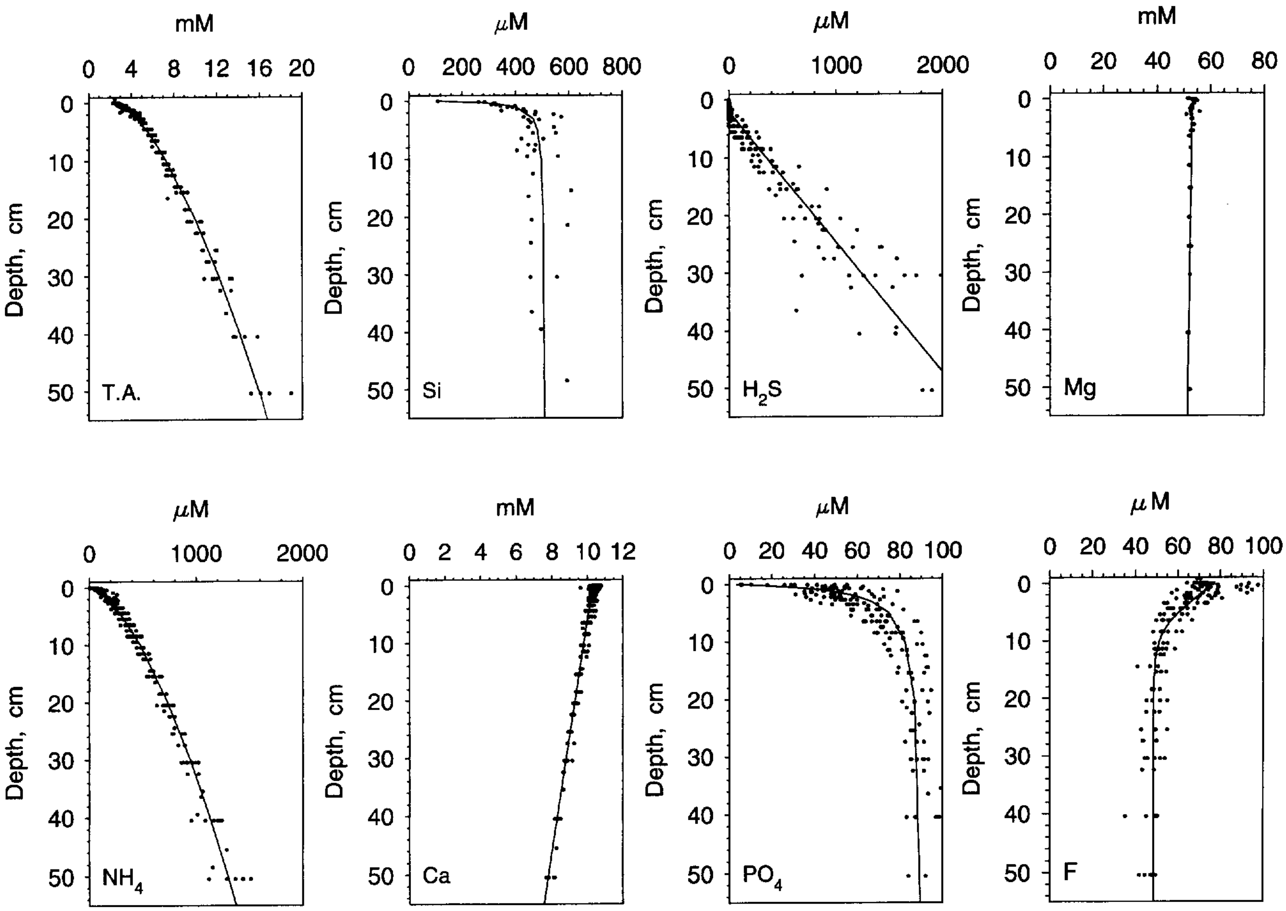


FIG. 9. Composite profiles of porewater total alkalinity, silica, hydrogen sulfide, ammonia, Ca, and phosphate taken from all the box cores analyzed. Phosphate data from BC78 and 82 are omitted. The curves through each plot represent best fits of simple functions to these data. These curves may be written as TA (mM) = $1.13x^{0.633} + 2.41$, where $x$ = depth in centimeters; Si ($\mu$M) = $((400x)/(0.378 + x)) + 110$; $H_2S$ ($\mu$M) = $44.2(x - 2.02)$; $NH_4$ ($\mu$M) = $114x^{0.622}$; Ca (mM) = $-0.0497x + 10.3$; $PO_4$ ($\mu$M) = $((88.0x/(1.19 + x)) + 3.70$; Mg (mM) = $-0.030x + 53.14$; and F ($\mu$M) = $37.5/(1 + e^{.355(x-2.97)}) + 48.57$.

$$\mathrm{TA} = [\mathrm{HCO_3}] + 2[\mathrm{CO_3}] + [\mathrm{B(OH)_4}] + [\mathrm{OH}] + [\mathrm{HPO_4}] + 2[\mathrm{PO_4}] + [\mathrm{SiO(OH)_3}] + [\mathrm{HS}] + [\mathrm{NH_3}] - [\mathrm{H_T}] - [\mathrm{H_3PO_4}];$$

and computed carbonate alkalinity and its components according to

$$\mathrm{CA} = \mathrm{TA} - [K_B\Sigma B/([\mathrm{H_T}] + K_b] - [K_{Si}\mathrm{Si}/([\mathrm{H_T}] + K_{Si}] - [\Sigma \mathrm{PO_4}(1/([\mathrm{H_T}]^2/K_{P1}*K_{P2} + [\mathrm{H_T}]/K_{P2} + 1 + K_{P3}/[\mathrm{H_T}]) + 2/([\mathrm{H_T}]^3/(K_{P1}*K_{P2}*K_{P3}) + [\mathrm{H_T}]^2/(K_{P2}*K_{P3}) + [\mathrm{H_T}]/K_{P3} + 1) - 1/(1 + K_{P1}/[\mathrm{H_T}] + K_{P1}*K_{P2}/[\mathrm{H_T}]^2 + K_{P1}*K_{P2}*K_{P3}/[\mathrm{H_T}]^3))] - [K_w(\mathrm{FH})/[\mathrm{H_T}] - [\mathrm{H_T}]/(\mathrm{FH})] - [\Sigma \mathrm{H_2S}/[\mathrm{H_T}]/K_{s1} + 1)] - [\Sigma \mathrm{NH_4}/(1 + [\mathrm{H_T}]/K_N)],$$

where all equilibrium constants are stoichiometric constants and FH is a formulation for the activity of $H^+$ in seawater. This allowed carbonate ion concentrations to be computed as

$$[\mathrm{CO_3^{2-}}] = \mathrm{CA}/(2 + K_2[\mathrm{H_T}]),$$

where $K_2$ is the second stoichiometric dissociation constant for carbonic acid, which was calculated for the in situ temperature, salinity, and pressure to equal $5.80 \times 10^{-10}$.

Possible measurement errors in pH due to electrode drift or overestimation of its response slope in this case are estimated to be ±0.03 pH units SWS (Fig. 10) which is less than apparent spatial variations. Our approximations of TA and other species such as Ca or fluoride as functions of depth may include pressure artifacts (Murray et al., 1980) and have sample acquisition errors one can scale based on the curve fitting in Fig. 9.

In spite of these uncertainties, our calculations suggest that the porewaters of the Santa Barbara Basin become saturated with respect to both CFA and calcite within the first 0.25 mm of the sediment (Fig. 14). The variable that exerts the greatest control on the outcome of these calculations is pH for its influence on phosphate and carbonate ion activi-

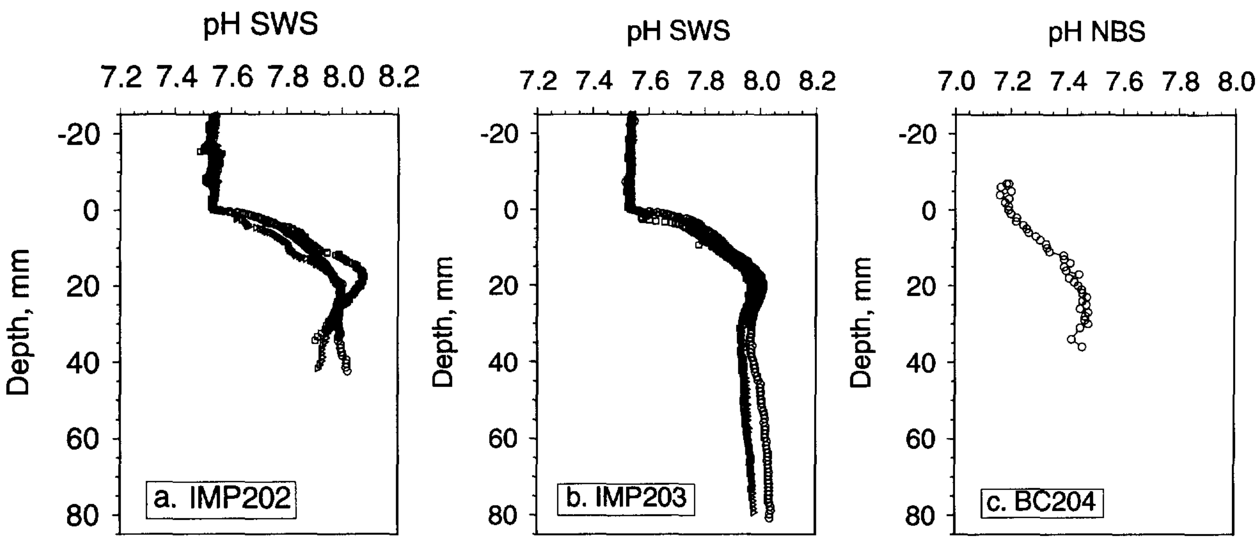


FIG. 10. Microelectrode pH profiles in SBB sediments. (a) Three in situ profiles. During this deployment the microprofiler's tripod released before profiling was completed. (b) Three complete in situ microprofiles. Each sensor was retracted after profiling and read in the bottom water. These readings correspond to within ±0.025 pH units of the mean bottom water readings before the sensors entered the sediment. (c) A shipboard profile measured in a chilled core.

ties. At and below 2 cm depth, supersaturation factors for CFA are very similar to those calculated by Ruttenberg and Berner (1993) for Long Island Sound sediments.

### 4.2. Porewater Profiles, Fluxes, and Rates of Authigenic Mineral Formation

Ruttenberg and Berner (1993) were able to detect an increase in authigenic P below the surface of Long Island Sound sediments via a sequential leaching procedure, but since 10-cm sections of sediment were homogenized for these analyses, it was not certain whether this P was taken up throughout the sediment-column or near the sediment–water interface. The details of our porewater profiles from the Santa Barbara Basin suggest there is unsteady uptake of phosphate and fluoride into solid phases within the uppermost 5–10 cm of these sediments but not below. Major reactions that could account for both $PO_4^{3-}$ and $F^-$ uptake are incorporation into precipitating carbonate fluorapatite (or a precursor phase, Gulbrandsen et al., 1984), incorporation into precipitating $CaCO_3$, or adsorption by sediment particles due to pH and other changes in porewater chemistry (Rude and Aller, 1994).

Support for transient CFA precipitation comes from the observation that, in box cores 21, 61, and 68, at least (Fig. 4), the depths which mark inflexion points in $\Sigma PO_4^{3-}$ and $F^-$ profiles coincide. Van Cappellan and Berner (1988) use a diagenetic model to predict that dissolved P and F profiles will show inflexion points at the base of a layer of preferential CFA precipitation. If precipitation within this layer occurs only within fixed depth limits and is short-lived due to nonsteady state conditions and/or rapid burial, and if diagenesis proceeds without CFA precipitation outside the layer, the Van Cappellan and Berner (1988) model also shows that P-enrichment may be undetectable in the solid phase. (One can set appropriate limits for the integrals in Eqns. 13 or 28 from Van Cappellan and Berner (1988) and predict that authigenic P concentrations should be less than 0.1% by dry weight for a sedimentation rate equal to 0.4 cm $yr^{-1}$ and dissolved phosphate concentrations which correspond to the SBB).

Co-adsorption might produce corresponding dissolved P and F depletions, but this argument may be one of semantics since adsorption on incipient surfaces must be the first step in CFA precipitation. Ferric iron oxyhydroxides, the minerals most likely to coadsorb P and F are readily reduced in

Table 2. Measured Bottom Water Characteristics of the Basin Determined from Collections November 7, 1993

| Collection | Water Depth, m | $TCO_2$ µmol $kg^{-1}$ | TA µmol $kg^{-1}$ | $O_2$ µmol $kg^{-1}$ | $NO_3$ µmol $kg^{-1}$ | Si µmol $kg^{-1}$ | $PO_4$ µmol $kg^{-1}$ | Salinity |
|---|---|---|---|---|---|---|---|---|
| Hydrocast | 589* | 2344.4 | 2354.9*** | 1.5 | 22.0 | 107.4 | 3.59 | 34.223 |
| Hydrocast | 583* | 2345.0 | 2339.6*** | 1.3 | 21.3 | 107.2 | 3.61 | 34.228 |
| IMP203 Niskin | 590** | 2345.6 | n.d. | n.d. | n.d. | n.d. | n.d. | 34.230 |

* based on reversing thermometer, data for the entire water column can be obtained from C. Reimers, **PDR depth of deployment location, *** average of duplicate determinations, n.d. indicates not determined

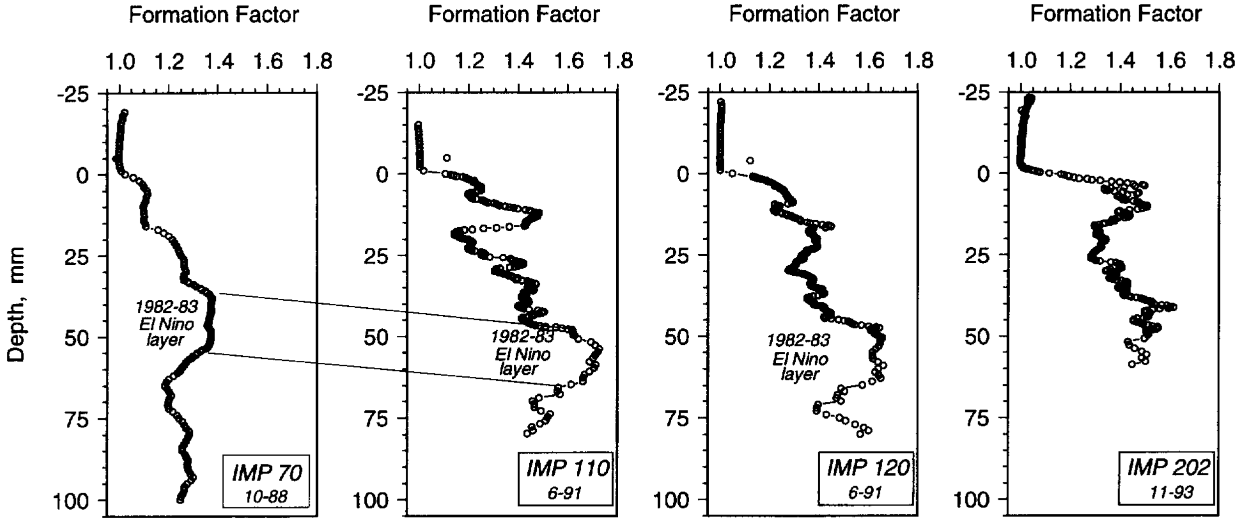


FIG. 11. Formation factor profiles in Santa Barbara Basin sediments designated by microprofiler deployment. Filled circles represent readings taken after the resistivity probe was returned to bottom water (IMP 70, 110, and 120 only). Since the sensor recorded relatively high values in the water after profiling during the 1991 experiments, the formation factor values near the base of these profiles are suspected to be 0.1–0.2 units higher than true values. Burial of a sediment layer that was deposited during 1982–83 can be followed between the 1988 and 1991 profiles. This layer was deeper than the bottom of the 1993 profile.

SBB sediments (Fig. 6) and so they can not act as a lasting sink.

Fluoride and phosphate could adsorb to or become incorporated into calcite precipitating in the first few centimeters of sediment, but fluoride and calcium flux estimates suggest this can not be the major sink for F. The composite $F^-$ profile in Fig. 9 illustrates that the maximum rate of decrease in fluoride occurs most often at 3.0 cm. The fluoride gradient predicted by the composite profile at 3 cm, $dC/dz = 3.3 \pm 1.0$ $\mu$mol cm$^{-4}$, suggests a localized fluoride uptake rate of $-0.64 \pm 0.19$ $\mu$mol cm$^{-2}$ y$^{-1}$ assuming

$$J_F = \frac{D_0}{F_f}\frac{dC}{dz},$$

where $D_0 = 250$ cm$^2$y$^{-1}$ at 6°C (Li and Gregory, 1974), and $F_f = 1.3$, the formation factor at 3 cm. Assuming a fluoride content of 1000 ppm in calcium carbonate (Rude and Aller, 1994), this fluoride flux would demand an uptake rate of Ca equal to roughly $-130$ $\mu$mol cm$^{-2}$ y$^{-1}$, if fluoride was removed only into authigenic $CaCO_3$. The calcium removal rate predicted by the extended, porewater Ca gradient (Fig. 9) is only $-5.7 \pm 0.2$ $\mu$mol cm$^{-2}$ y$^{-1}$, and there is indication of only a slight enhancement of this gradient near the sediment surface.

If the fluoride flux is assumed to signal removal into authigenic CFA, $(Ca_{9.54}Na_{0.33}Mg_{0.13}(PO_4)_{4.8}(CO_3)_{1.2}(F)_{2.48})$, the corresponding calcium uptake rate should equal $-2.5 \pm 0.7$ $\mu$mol cm$^{-2}$ y$^{-1}$ and phosphorus should be removed at $-1.2 \pm 0.4$ $\mu$mol cm$^{-2}$ y$^{-1}$. This calcium removal rate is well within limits set by the dissolved Ca profiles, and the phosphate flux approaches the burial rate of inorganic P (1.6 $\mu$mol cm$^{-2}$ y$^{-1}$, assuming 0.1% P and an average sediment accumulation rate of 51 mg cm$^{-2}$ y$^{-1}$; Schmidt and Reimers, 1991).

In short, the porewater profiles of dissolved F, P, and Ca when analyzed together are consistent with the interpretation that CFA, or a less crystalline precursor with a similar composition, is forming in the uppermost sediments, followed by authigenic calcite precipitation that is not depth specific but is responsible for removing an overall calcium flux on the order of 6 $\mu$mol cm$^{-2}$ y$^{-1}$. This rate of calcite precipitation would increase inorganic C concentrations by 0.1% on average, an amount expected to be masked by the variability in the accumulation of biogenic calcite.

The porewater evidence that authigenic precipitation of P, F, Ca, and inorganic C occurs, but is not readily apparent in solid phase profiles from the SBB, suggests that other rapidly accumulating sediments may be sinks for these elements (Ruttenberg, 1993). In magnitude, the estimates of P and F fluxes into the SBB sediments are analogous to environments with known modern phosphorites such as the margins of Peru and Mexico (Froelich et al., 1988; Schuffert et al., 1994). The primary difference between the SBB and these other margin environments is sedimentation rate. Sites with phosphorites off Peru and Mexico, typically have average sedimentation rates of 0.002–0.03 cm y$^{-1}$ (Kim and Burnett, 1988; Schuffert et al., 1994), and these rates are markedly discontinuous. The SBB sedimentation rate is 10–200 times higher and very steady.

But why should CFA precipitation be limited to the uppermost few centimeters of the sediment column, if it occurs at all in the SBB?

Thermodynamically it appears the precipitation of both CFA and calcite is favorable, and nonsteady state changes in porewater solutes, that were not taken into account in our

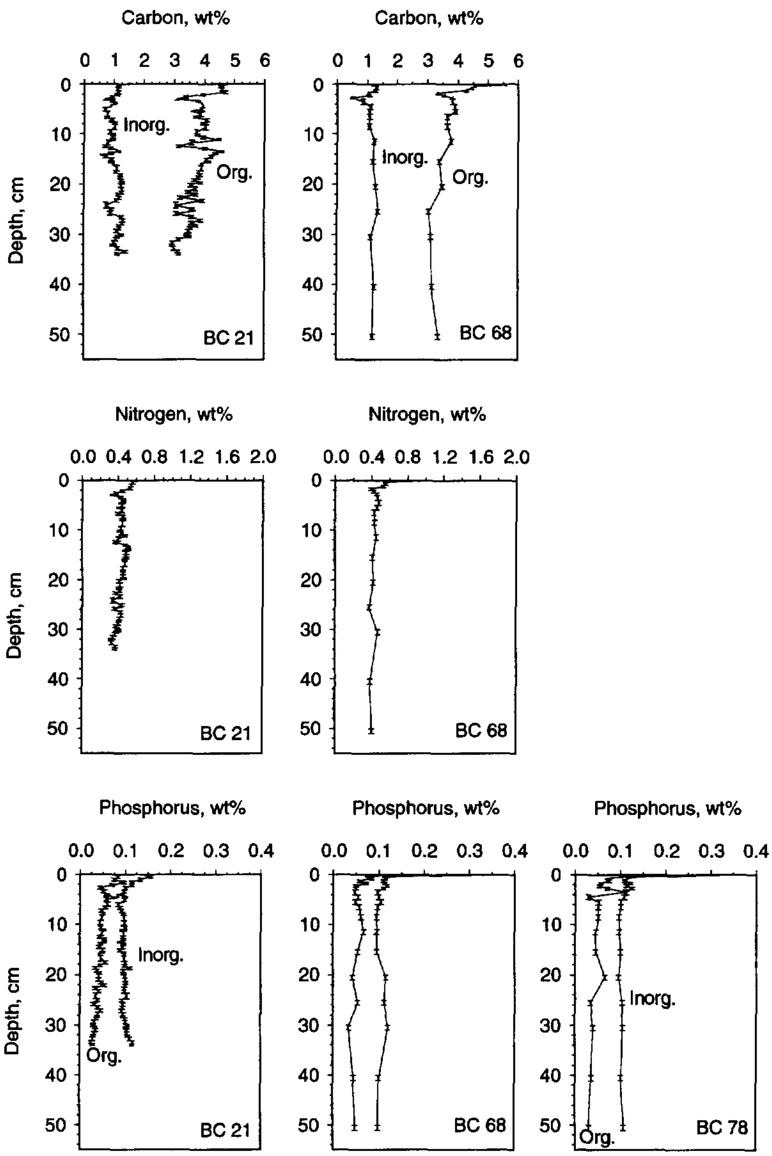


FIG. 12. Profiles of organic and inorganic carbon, total N, and organic and inorganic P. All concentrations are plotted in % dry weight of total salt-free sediment. Box core 21 was sampled over its entire length, layer by layer according to color changes. Vertical bars indicate the thicknesses of the sampled intervals.

saturation state analysis, are unlikely to lead to periods of undersaturated conditions for either mineral. Therefore, as Glenn and Arthur (1988) argued, the ultimate limiting factor in CFA growth may be an inability of this mineral to accommodate increasing carbonate substitution at higher carbonate ion concentrations in porewaters. Figure 14 shows that $CO_3^{2-}$ concentrations do increase below the usual depth interval (~1–5 cm) where dissolved P and F depletions may signal CFA precipitation in the SBB. However, this increase is gradual and does not suggest there should be an abrupt change in CFA stability.

Calcite supersaturation has been observed as a common feature of anoxic sediments and attributed to lack of a suitable substrate or the presence of inhibitors such as Mg, or organic compounds that retard mineral nucleation (Gaillard et al., 1989). It is likely CFA precipitation is impeded by similar factors (Burnett, 1977; Glenn and Arthur, 1988; Van Capellen and Berner, 1990) especially when precipitates form as small interstitial particles rather than as coatings on preexisting hard substrates. For this reason we suspect that if the precipitation of CFA is to proceed within specific horizons of organic-rich sediments, extraneous nuclei must be introduced. In the uppermost centimeters of SBB sediments, two sources of nuclei may be *Beggiatoa* filaments or redox reactions involving Fe and S. The former are known to contain intracellular inclusions of elemental S and polyphosphate (Strohl, 1989), whereas the latter are certain to form colloids of $Fe(OH)_3$, $S^0$ and/or FeS. The fresh inter-

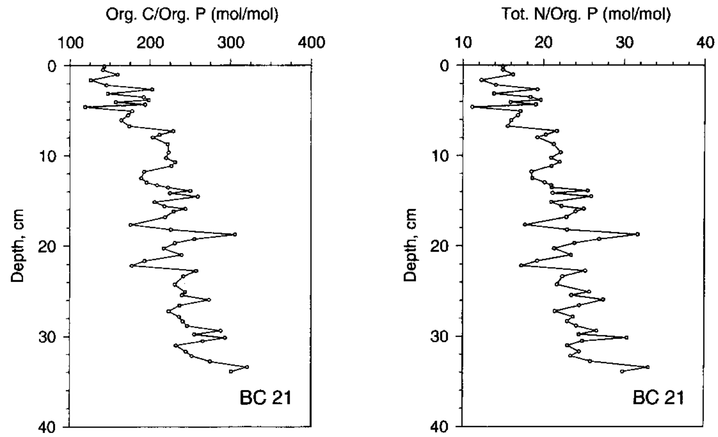


FIG. 13. Downcore changes in solid phase ratios.

faces of such microbial or colloidal substances could trigger the precipitation of CFA, or an amorphous precursor, from the supersaturated pore solutions. In deeper sediments where $HS^-$ accumulates in the porewaters, the *Beggiatoa* and Fe or S colloids should not be present. Authigenic calcite on the other hand, may precipitate away from the sediment interface because carbonate microfossils serve as growth surfaces. The evidence which suggests this explanation is the observation that phosphate minima occur always above the first interval with detectable dissolved sulfide in cores where the sulfide gradient does not extend to the sediment–water interface.

### 4.3. Iron Cycling and Phosphate and Fluoride Desorption

Figures 4, 5, and 6 indicate that Fe cycling exerts a strong control on the dissolved sulfide concentrations in the uppermost sediments of the SBB. Iron oxyhydroxides are quickly reduced by microorganisms and by reaction with $HS^-$, producing porewater $Fe^{2+}$ and liberating excess $PO_4^{3-}$ and $F^-$. The $PO_4^{3-}$ and $F^-$ presumably adsorbed to the Fe oxyhydroxides in the water column (Shiller et al., 1985; Froelich et al., 1988; Rude and Aller, 1994). Shiller et al. (1985) comment that perhaps the most distinctive feature of Santa Barbara Basin particulate geochemistry is the Fe enrichment in deeper samples (from the water column). Since concentrations of Fe(III) phases in the first two centimeters of the sediments are replaced by equal concentrations of Fe(II) minerals below 2 cm (Fig. 6), it appears little diagenetic Fe(III) enrichment occurs. That is, instead of being transported toward the sediment surface and reoxidized to any significant degree, porewater $Fe^{2+}$ is sequestered mostly into sulfide minerals, and these minerals are buried in sediments that have been accumulating for only about 5 years. Since there is no bioturbation to enhance the recycling of Fe between the surface oxic and subsurface anoxic zone, Fe recycling is not fast enough to dominate over sulfate reduction in anaerobic C oxidation (Table 3) (Canfield et al., 1993). The zone where the sulfate reduction rate is maximum falls between 2 and 4 cm depth. Here, porewater $Fe^{2+}$ becomes depleted, porewater sulfide is kept low by reaction with $Fe^{2+}$, and pH decreases slightly. These porewater features mark this as the horizon of maximum monosulfide precipitation and gradual pyritization (Gagnon et al., 1995). Without the burial of Fe(III) phases, depletions in porewater $PO_4^{3-}$ and $F^-$ are not expected to be caused solely by adsorption reactions.

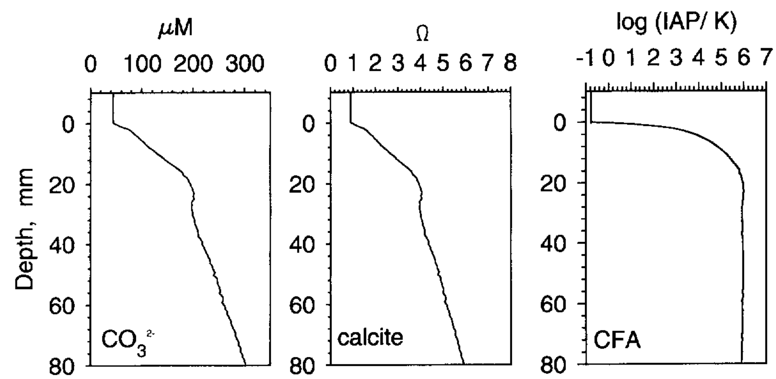


FIG. 14. Carbonate ion concentration, the degree of calcite saturation, and the ratio of the Ion Activity Product to solubility product for CFA as a function of depth in SBB sediments.

Table 3. Carbon Oxidation Rates (μmol $cm^{-2}$ $y^{-1}$) by Iron and Sulfate Reduction in the SBB.

| | |
|---|---|
| Iron Reduction[1] | 5.7 |
| Sulfate Reduction[2] | 156 |

[1] computed assuming a simple steady state diffusion and reaction model wherein an average $Fe^{2+}$ production rate estimate is made by fitting an exponential function to the uppermost points of all the pore water $Fe^{2+}$ profiles combined with with organic carbon/Fe stoichiometry equal to 0.25 as in Reimers et al. (1992).
[2]computed by summing sulfate reduction rate measurements (Figure 6) from 0-38 cm and assuming a C/S stoichiometric ratio equal to 2.

### 4.4. Processes Determining Porewater pH

We have inferred that the sediment biogeochemistry in the Santa Barbara Basin drives shallow AVS accumulation, pyritization, and CFA precipitation, and favors dispersed authigenic calcite formation. We have also seen overlap between zones where the different pathways of organic matter decomposition consume oxidants. All of these reactions are reflected in the pH of the porewaters. Until recently, there has been little reliable porewater pH data from organic-rich sediments. Porewaters in the SBB have pH values that always exceed bottom water values. This result we believe is an indication of a system dominated early by iron liberation reactions. As shown in Table 4 and by the modeling examples in Boudreau and Canfield (1988), the Fe liberating reactions consume protons and liberate other cations. This effect of Fe liberation may be buffered by FeS and $CaCO_3$ precipitation (Table 4), but in the SBB, FeS, and $CaCO_3$ precipitation reactions do not appear to dictate the porewater chemistry at depths above 2 cm.

We can also contrast our SBB porewater pH profiles to profiles from other sediments we have studied to evaluate if the anoxic porewaters of the SBB are unusually alkaline. In Fig. 15 are plotted pH-depth profiles from San Clemente Basin and Santa Monica Basin, two other basins in the California Borderlands. The San Clemente Basin differs from SBB principally because it has higher bottom water oxygen concentrations ($\sim$60 $\mu$M), and its sediments are bioturbated (see Bender et al., 1989, and Shaw et al., 1990, for an overview of the porewater chemistry in this basin). Dissolved oxygen penetrates to 7 or 8 mm (Reimers, 1987), Mn and Fe peak between 2 and 6 cm, and sulfide is not detectable until approximately 25 cm (Shaw et al., 1990; K. Ruttenberg, unpubl. data). The Santa Monica Basin is usually as oxygen depleted as the SBB (the bottom water $O_2$ concentration was measured as 8.2 $\mu$M when the pH profile in Fig. 15 was measured). Its sediments show little indication of mixing (Finney and Huh, 1989), and they are enriched in Fe (up to 3.5 wt% leachable Fe, Shaw et al., 1990). Sedimentation rates are 0.07 cm $y^{-1}$ (Bruland et al., 1974) compared to the rate of roughly 0.4 cm $y^{-1}$ we have reconfirmed for the Santa Barbara Basin. Sulfide is detectable in the first 0.25 cm of sediment of Santa Monica Basin, but it remains at levels of 9–20 $\mu$M to at least 20 cm depth (K. Ruttenberg unpubl. data). Porewater $Fe^{2+}$ may reach concentrations >200 $\mu$M and remain >100 $\mu$M to at least 50 cm (Jahnke, 1990; Shaw et al., 1990).

In the San Clemente Basin sediments, porewater pH is lowered immediately below the sediment–water interface in response to the oxic degradation of organic matter and the oxidation of reduced byproducts of nitrate, Mn, Fe, and sulfate reduction reactions that are transported to the oxic zone. Reactions affecting the oxic zone have been described and modeled by Boudreau (1987), Boudreau and Canfield (1993), and Van Cappellen and Wang (1996). The general shape of this pH profile looks very much as these models predict. Below the oxic zone, pH increases as it does within the first 2 cm of the SBB, but the pH-value reached at depth is only about 7.8.

Table 4. Examples of Dissolution and Precipitation Reactions Involving Iron which Govern pH in Anoxic Pore Waters (after Boudreau and Canfield, 1988)

1) Iron Liberation:

$$4FeOOH + CH_2O + H_2O \rightarrow 4Fe^{2+} + HCO_3^- + 7OH^-$$

$$2Fe(OH)_3 + HS^- + 5H^+ \rightarrow 2Fe^{2+} + 6H_2O + S^0$$

$$2FeOOH + HS^- + 5H^+ \rightarrow 2Fe^{2+} + 4H_2O + S^0$$

$$2Fe_2O_3 + HS^- + 5H^+ \rightarrow 2Fe^{2+} + 3H_2O + S^0$$

$$FeFe_2O_4 + HS^- + 7H^+ \rightarrow 3Fe^{2+} + 4H_2O + S^0$$

$$KMgFe_2AlSi_3O_{10}(OH)_8 + 7H^+ + ½ H_2O \rightarrow K^+ + Mg^{2+} + 2Fe^{2+} + ½ Al_2Si_2O_5(OH)_4 + 2H_4SiO_4$$

$$Mg_2Fe_3Al_2Si_3O_{10}(OH)_8 + 10H^+ \rightarrow 2Mg^{2+} + 3Fe^{2+} + Al_2Si_2O_5(OH)_4 + H_4SiO_4 + 5H_2O$$

2) Monosulfide Precipitation:

$$Fe^{2+} + HS^- \rightarrow FeS(s) + H^+$$

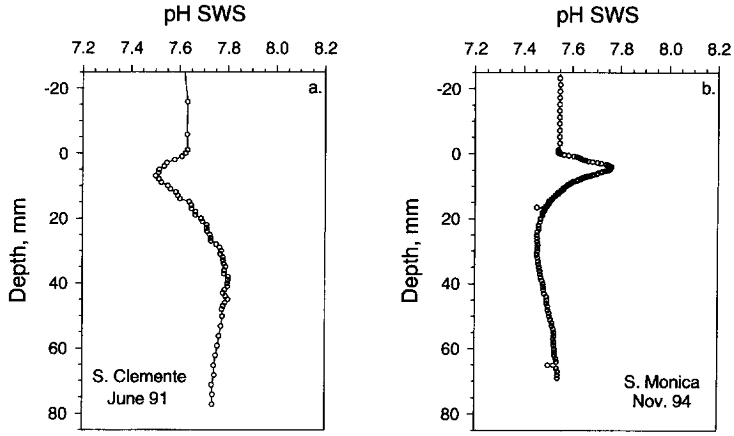


FIG. 15. In situ pH porewater profiles measured with microelectrodes in (a) San Clemente Basin, June 1991, water depth = 1935 m; and (b) Santa Monica Basin, November 1994, water depth = 900 m. After profiling, both microelectrodes were read in the overlying bottom waters again, and these readings agreed to better than 0.01 pH units with readings before the sensors entered the sediment. Bottom water pH values were calculated from measurements of the TA and $TCO_2$ of the bottom water.

In Santa Monica Basin, pH appears to be first raised in association with rapid rates of microbial mediated organic matter oxidation and iron liberation, as it is in the SBB, but then it decreases dramatically (see Jahnke, 1990, for pH profiles of similar shape determined in cores from Santa Monica). In this case it appears that the effects of iron sulfide or carbonate precipitation on pH are greater (below about 5 mm) than the effects of Fe liberation reactions. Another possible explanation is that Fe is released to a significant degree by cation exchange reactions that do not consume organic matter or protons. Sholkovitz (1973) proposed that cation exchange by clays in Santa Barbara Basin sediments was responsible for the observed depletion of $Mg^{2+}$. This process may be even more pronounced in Santa Monica. Only a suitably complete dataset, similar to what this study provides for the Santa Barbara Basin, and modeling will resolve this uncertainty. At this point we wish only to conclude that anoxic sediments can have widely different porewater pH profiles. Such profiles have helped to reveal the signature of authigenic mineral formation in the Santa Barbara Basin.

## 5. CONCLUDING REMARKS

The data presented in this study indicate that the SBB conforms to a model of mineral paragenesis wherein CFA accumulation is restricted to the near-surface of organic-rich sediments. In such surface sediments, a critical factor is that iron oxyhydroxides are reduced, which raises pH and releases sorbed phosphate, fluoride, and $Fe^{2+}$. The $Fe^{2+}$ is then available to sequester dissolved sulfide into FeS, leading to pyrite formation. Also, colloidal precipitates of iron or sulfur, or fresh bacterial products are suggested to supply surfaces which may initiate CFA precipitation. In sulfide-rich layers, these nuclei should not be as readily available. Thus, CFA precipitation occurs only in the first ~5 cm of sediment, and calcite precipitation removes $CO_3^{2-}$ and $Ca^{2+}$ ions from deeper porewaters.

Sedimentation rates for the SBB Basin were reconfirmed as equal to 4.2 ± 0.4 mm $y^{-1}$ by tracing the progressive burial of a layer with relatively high formation factor values. These rapid burial rates obscure solid phase evidence for authigenic CFA and calcite, in spite of porewater-based fluxes of $F^-$ which predict CFA accumulation rates within the range of those determined in regions of modern phosphorite formation. The SBB appears, therefore, to represent another example of CFA formation in a terrigenous-rich sediment which does not reside in the classic slope environment described for phosphorite formation. Painstaking separations of authigenic P from these sediments (after Ruttenberg and Berner; 1993) are needed as a second level of proof for CFA formation.

Finally, because the SBB sediments are not bioturbated and are enriched in Fe, their pH, which rises above 8.0 (SWS), may represent an endmember for pH values in anoxic sediments. The value of in situ pH microelectrode measurements is that they provide a very sensitive recording of the rapid changes that occur in the interface zone of porewater systems. They also greatly improve our ability to determine thermodynamic constraints on reactions affecting those systems.

*Acknowledgments*—This work was supported by NSF grants OCE87-14996 and OCE94-96066 to C. Reimers. Helpful reviews from A. Mucci, J. McManus, and four anonymous reviewers helped shape the paper's discussion. We thank Tom Brown, Bernie Boudreau, Jim Leather, Guy Emanuele, Sue Boehme, Marilyn Mayer, Jim Bauer, Malana Tabak, Wei-Jun Cai, and Gordy Zimm for assistance either at sea or in the laboratory. We are also grateful to the Resident Technicians at Scripps Institution of Oceanography and the Captains and crews of the R/Vs *R. G. Sproul* and *New Horizon* for helping us make it all happen.

*Editorial handling:* B. P. Boudreau

## REFERENCES

Aspila K. I., Agemian H., and Chau A. S. Y. (1976) A semi-automated method for the determination of inorganic, organic and total phosphate in sediments. *Analyst* **101,** 187–197.

Bender M. et al. (1989) Organic carbon oxidation and benthic nitrogen and silica dynamics in San Clemente Basin, a continental borderland site. *Geochim. Cosmochim. Acta* **53**, 685–699.

Boudreau B. P. (1987) A steady-state diagenetic model for dissolved carbonate species and pH in the porewaters of oxic and suboxic sediments. *Geochim. Cosmochim. Acta* **51**, 1985–1996.

Boudreau B. P. and Canfield D. E. (1988) A provisional diagenetic model for pH in anoxic porewaters: Application to the FOAM site. *J. Mar. Res.* **46**, 429–455.

Boudreau B. P. and Canfield D. E. (1993) A comparison of closed- and open-system models for porewater pH and calcite-saturation state. *Geochim. Cosmochim. Acta* **57**, 317–334.

Bradshaw A. L. and Brewer P. G. (1988) High precision measurement of alkalinity and total carbon dioxide in seawater by potentiometric titration—I. presence of unknown protolyte(s)? *Mar. Chem.* **23**, 69–86.

Brewer P. G. and Spencer D. W. (1971) Colorimetric determination of manganese in anoxic waters. *Limnol. Oceanogr.* **16**, 107–118.

Bruland K. W., Bertine K., Koide M., and Goldberg E. D. (1974) History of metal pollution in Southern California coastal zone. *Environ. Sci. Technol.* **8**, 425–432.

Burnett W. C. (1977) Geochemistry and origin of phosphorite deposits from off Peru and Chile. *Geol. Soc. Amer. Bull.* **88**, 813–823.

Cai W.-J. (1992) In situ microelectrode studies of the early diagenesis of organic carbon and $CaCO_3$ in hemipelagic sediments of the northeast Pacific Ocean. PhD thesis, Univ. California.

Cai W.-J. and Reimers C. E. (1993) The development of pH and $pCO_2$ microelectrodes for studying the carbonate chemistry of porewaters near the sediment-water interface. *Limnol. Oceanogr.* **38**, 1776–1787.

Canfield D. E. (1988) Sulfate reduction and the diagenesis of iron in anoxic marine sediments. Ph.D. thesis, Yale Univ.

Canfield D. E. (1989) Reactive iron in marine sediments. *Geochim. Cosmochim. Acta* **53**, 619–632.

Canfield D. E. and Raiswell R. (1991) Pyrite formation and fossil preservation. In *Taphonomy: Releasing the Data Locked in the Fossil Record* (ed. P. A. Allison and D. E. G. Briggs); *Topics Geobiol.* **9**, 337–387.

Canfield D. E., Thamdrup B., and Hansen J. W. (1993) The anaerobic degradation of organic matter in Danish coastal sediments: iron reduction, manganese reduction, and sulfate reduction. *Geochim. Cosmochim. Acta* **57**, 3867–3884.

Cline J. D. (1969) Spectrophotometric determination of hydrogen sulfide in natural waters. *Limnol. Oceanogr.* **14**, 454–458.

Dickson A. G. and Millero F. (1987) A comparison of the equilibrium constants for the dissolution of carbonic acid in seawater media. *Deep-Sea Res.* **34**, 1733–1743.

Finney B. P. and Huh C-A. (1989) History of metal pollution in the Southern California Bight: An update. *Environ. Sci. Technol.* **23**, 294–303.

Fossing H. et al. (1995) Concentration and transport of nitrate by the mat-forming sulfur bacterium *Thioploca. Nature* **374**, 713–715.

Froelich P. N. et al. (1988) Early diagenesis of organic matter in Peru continental margin sediments: phosphorite precipitation. *Mar. Geol.* **80**, 309–343.

Gagnon C., Mucci A., and Pelletier E. (1995) Anomalous accumulation of acid-volatile sulphides (AVS) in a coastal marine sediment, Saguenay Fjord, Canada. *Geochim. Cosmochim. Acta* **59**, 2663–2675.

Gaillard J-F., Pauwels H., and Michard G. (1989) Chemical diagenesis in coastal marine sediments. *Oceanol. Acta* **12**, 175–187.

Gieskes J. M. (1969) Effect of temperature on the pH of seawater. *Limnol. Oceanogr.* **14**, 679–685.

Gieskes J. and Peretsman G. (1986) Water chemistry procedures aboard *Joides Resolution*—some comments. *Ocean Drill. Progr. Tech. Note 5*, Texas A&M Univ.

Glenn C. R. and Arthur M. A. (1988) Petrology and major element geochemistry of Peru margin phosphorites and associated diagenetic minerals: authigenesis in modern organic-rich sediments. *Mar. Geol.* **80**, 231–268.

Glenn C. R., Arthur M. A., Yeh H.-W., and Burnett W. C. (1988) Carbon isotopic composition and lattice-bound carbonate of Peru-Chile margin phosphorites. *Mar. Geol.* **80**, 287–308.

Grant C. W. (1991) Distributions of bacterial mats (*Beggiatoa* spp.) in Santa Barbara Basin, California: A modern analog for organic-rich facies of the Monterey Formation, Master's thesis, Calif. State Univ. Long Beach.

Greenhalgh R. and Riley J. P. (1961) The determination of fluorides in natural waters with particular reference to seawater. *Anal. Chim. Acta* **25**, 179–188.

Gulbrandsen R. A., Roberson C. E., and Neil S. T. (1984) Time and the crystallization of apatite in seawater. *Geochim. Cosmochim. Acta* **48**, 213–218.

Hansson I. (1973) A new set of pH-scales and standard buffers for sea water. *Deep-Sea Res.* **20**, 479–491.

Hülsemann J. and Emery K. O. (1961) Stratification in recent sediments of Santa Barbara Basin as controlled by organisms and water character. *J. Geol.* **69**, 279–290.

Jahnke R. A. (1990) Early diagenesis and recycling of biogenic debris at the seafloor, Santa Monica Basin, California. *J. Mar. Res.* **48**, 413–436.

Jahnke R. A., Emerson S. R., Roe K. K., and Burnett W. C. (1983) The present day formation of apatite in Mexican continental margin sediments. *Geochim. Cosmochim. Acta* **47**, 259–266.

Johnson K. M., King A. E., and Sieburth J. M. (1985). Coulometric $TCO_2$ analyses for marine studies; and introduction. *Mar. Chem.* **16**, 61–82.

Johnson K. M., Sieburth J. M., Williams P. J. L., and Bränström L. (1987) Coulometric total carbon dioxide analysis for marine studies: automation and calibration. *Mar. Chem.* **21**, 117–133.

Jørgensen B. B. (1978) A comparison of methods for the quantification of bacterial sulfate reduction in coastal marine sediments I. Measurement with radiotracer techniques. *Geomicrobiol. J.* **1**, 11–27.

Kim K. H. and Burnett W. C. (1988) Accumulation and biological mixing of Peru margin sediments. *Mar. Geol.* **80**, 181–194.

Koide M., Soutar A., and Goldberg E. D. (1972) Marine geochronolgy with $^{210}$Pb. *Earth Planet. Sci. Lett.* **14**, 442–446.

Li Y.-H. and Gregory S. (1974) Diffusion of ions in sea water and in deep-sea sediments. *Geochim. Cosmochim. Acta* **38**, 703–714.

Lynn R. J. and Simpson J. J. (1987) The California Current system: The seasonal variability of its physical characteristics. *J. Geophys. Res.* **92**, 12,947–12,966.

Millero F. J. (1979) The thermodynamics of the carbonate system in seawater. *Geochim. Cosmochim. Acta* **43**, 1651–1661.

Millero F. J. and Schreiber D. R. (1982) Use of the ion pairing model to estimate activity coefficients of the ionic components of natural waters. *Amer. J. Sci.* **282**, 1508–1540.

Mucci A. (1983) The solubility of calcite and aragonite in seawater at various salinities, temperatures and one atmosphere total pressure. *Amer. J. Sci.* **283**, 789–799.

Murray J. W., Emerson S. R., and Jahnke R. A. (1980) Carbonate saturation and the effect of pressure on the alkalinity of interstitial waters from the Guatemala Basin. *Geochim. Cosmochim. Acta* **44**, 963–972.

Olmez I., Sholkovitz E. R., Hermann D., and Eganhouse R. P. (1991) Rare earth elements in sediments off southern California: a new anthropogenic indicator. *Environ. Sci. Technol.* **25**, 310–316.

Park P. K. (1969) Oceanic $CO_2$ system: an evaluation of ten methods of investigation. *Limnol. Oceanogr.* **14**, 179–186.

Pedersen T. F. (1979) The geochemistry of sediments of the Panama Basin, eastern equatorial Pacific Ocean. Ph.D. thesis, Univ. Edinburgh.

Reimers C. E. (1987) An in situ microprofiling instrument for measuring interfacial pore water gradients: Methods and oxygen profiles from the North Pacific Ocean. *Deep-Sea Res.* **34**, 2019–2035.

Reimers C. E., Lange C. B., Tabak M., and Bernhard J. M. (1990) Seasonal spillover and varve formation in the Santa Barbara Basin, California. *Limnol. Oceanogr.* **35**, 1577–1585.

Reimers C. E., Jahnke R. A., and McCorkle D. C. (1992) Carbon fluxes and burial rates over the continental slope and rise off

central California with implications for the global carbon cycle. *Global Biogeochem. Cycles* **6,** 199–224.
Rude P. D. and Aller R. C. (1994) Fluorine uptake by Amazon continental shelf sediment and its impact on the global fluorine cycle. *Cont. Shelf Res.* **14,** 883–907.
Ruttenberg K. C. (1992) Development of a sequential extraction method for different forms of phosphorus in marine sediments. *Limnol. Oceanogr.* **37,** 1460–1482.
Ruttenberg K. C. (1993) Reassessment of the oceanic residence time of phosphorus. *Chem. Geol.* **107,** 405–409.
Ruttenberg K. C. and Berner R. A. (1993) Authigenic apatite formation and burial in sediments from non-upwelling, continental margin sediments. *Geochim. Cosmochim. Acta* **57,** 991–1007.
Schimmelmann A., Lange C. B., and Berger W. H. (1990) Climatically controlled marker layers in Santa Barbara Basin sediments, and fine-scale core-to-core correlation. *Limnol. Oceanogr.* **35,** 165–173.
Schmidt H. and Reimers C. E. (1991) The recent history of trace metal accumulation in the Santa Barbara Basin, Southern California Borderland. *Estuarine Coastal Shelf Sci.* **33,** 485–500.
Schuffert J. D., Jahnke R., Kastner M., Leather J., Sturz A., and Wing M. R. (1994) Rates of formation of modern phosphorite off western Mexico. *Geochim. Cosmochim. Acta* **58,** 5001–5010.
Shaw T. J. (1989) An apparatus for fine-scale sampling of pore waters and solids in high porosity sediment. *J. Sediment. Petrol.* **59,** 633–634.
Shaw T. J., Gieskes J. M., and Jahnke R. A. (1990) Early diagenesis in differing depositional environments: the response of transition metals in porewater. *Geochim. Cosmochim. Acta* **54,** 1233–1246.
Shiller A. M., Gieskes J. M., and Price N. B. (1985) Particulate iron and manganese in the Santa Barbara Basin, California. *Geochim. Cosmochim. Acta* **49,** 1239–1250.
Sholkovitz E. (1973) Interstitial water chemistry of the Santa Barbara Basin sediments. *Geochim. Cosmochim. Acta* **37,** 2043–2073.
Soutar A. and Crill P. A. (1977) Sedimentation and climatic patterns in the Santa Barbara Basin during the 19th and 20th centuries. *Geol. Soc. Amer. Bull.* **88,** 1161–1172.
Stookey L. L. (1970) Ferrozine—a new spectrophotometric reagent for iron. *Anal. Chem.* **42,** 779–784.
Strohl W. R. (1989) *Beggiatoa.* In *Bergey's Manual of Systematic Bacteriology* (ed. J. G. Holt). Williams and Wilkins.
Tabatabai M. A. (1974) A rapid method for the determination of sulfate in water samples. *Environ. Lett.* **7,** 237–243.
UNESCO (1987) Thermodynamics of the carbon dioxide system in seawater. Reported by the carbon dioxide sub-panel of the joint panel on oceanographic tables and standards.
University of California Scripps Institution of Oceanography Data Reports, 1986, 1987, 1988, 1989, 1990, 1991, 1992, 1993 SIO references 86-9, 86-22, 87-7, 87-19, 88-8, 88-23, 89-2, 89-26, 90-19.
Van Cappellen P. and Berner R. A. (1988) A mathematical model for the early diagenesis of phosphorus and fluorine in marine sediments: apatite precipitation. *Amer. J. Sci.* **288,** 289–333.
Van Cappellen P. and Berner R. A. (1990) Crystal growth of marine apatite. In *Geochemistry of the Earth's Surface and Mineral Formation; 2nd International Symposium, Aix en Provence, France,* 331–333.
Van Cappellen P. and Wang Y. (1996) Cycling of iron and manganese in surface sediments: a general theory for the coupled transport and reaction of carbon, oxygen, nitrogen, sulfur, iron and manganese. *Amer. J. Sci.* **296,** 197–243.
Vetter R. D., Matrai P. M., Javor B., and O'Brien J. (1989) Reduced sulfur compounds in the marine environment analysis by high-performance liquid chromatography. In *Biogenic Sulfur in the Environment* (ed. E. S. Saltzman and W. J. Cooper); *Amer. Chem. Soc. Ser.* **393,** 243–261.
Westrich J. T. (1983) The consequences and controls of bacterial sulfate reduction in marine sediments. Ph.D. thesis, Yale Univ.

**Appendix A. Analytical methods applied to extracted porewater samples.**

| | CHEMICAL SPECIES | METHOD | PRECISION* | REFERENCE | BRIEF DESCRIPTION |
|---|---|---|---|---|---|
| 1. | $\Sigma PO_4$ | spectrophoto-metry | ±2% | Gieskes and Peretsman (1986) | Acidified samples were diluted with phosphate-free artificial seawater in volumes of 0.25:1.25 cm$^3$ (BC) or 0.1:1.4 cm$^3$ (K), respectively; standards (0-60 μM $\Sigma PO_4$) were diluted 0.5:1.0 cm$^3$; each 1.5 cm$^3$ of diluted sample or standard was combined with 2 cm$^3$ mixed reagent; resulting color read after 1 hour, in 1-cm cell, at 885 nm. |
| 2. | $\Sigma NH_4$ | spectrophoto-metry | ±2% | Gieskes and Peretsman (1986) | Non-acidified samples were diluted with bottom seawater or artificial seawater in volumes of 0.1:1 or 0.05:1.05 cm$^3$ (BC) or 0.025:1.075 cm$^3$ (K); standards (0-1000 μM $\Sigma NH_4$) were diluted 0.1:1 cm$^3$; each 1.1 cm$^3$ of diluted sample or standard was combined with 0.5 cm$^3$ phenol alchohol solution, 0.5 cm$^3$ sodium nitroprusside solution and 1 cm$^3$ oxidizing solution; color read after 1-4 hours, in a 1-cm cell at 640 nm. |
| 3. | $F^-$ | spectrophoto-metry | ±2% | Greenhalgh and Riley (1961) | 0.5 cm$^3$ aliquots of non-acidified samples and standards (0-80 μM $F^-$) were mixed with 0.25 cm$^3$ lanthanum-alizarin complexone reagent and read in a 1-cm cell, at 622 nm after 1 hour. |
| 4. | $\Sigma I$ | spectrophotometry | ±2% | adapted from Pedersen (1979) | 0.25 to 0.5 cm$^3$ samples or standards were combined with 0.04 cm$^3$ of bromine water and 1 cm$^3$ of acetate buffer (pH~5) and heated to ~80°C for 5 minutes. The samples were cooled and 0.04 cm$^3$ formic acid added to each. The samples were mixed, 0.03 cm$^3$ of 10%(by weight) KI solution and 0.5 cm$^3$ of 1% sulfamic acid solution were added to each and mixed again on a vortex mixer. Absorbance was measured at 355 nm in 1 cm cell exactly 3 minutes after the KI was added. |
| 5. | $Fe^{2+}$ | spectrophotometry | ±5% | Stookey (1970) | 1 cm$^3$ of acidified sample or standard (0-50 μM $Fe^{2+}$) was combined with 20λ each of acid reducer, ferrozine and buffer reagents; color read after several minutes in a 1-cm cell at 562 nm. |
| 6. | $Mn^{2+}$ | spectrophotometry | ±5% | Brewer and Spencer (1971) | Acidified samples and standards (0-50 μM $Mn^{2+}$) were diluted with artificial seawater in volumes of 0.5:2.5 and 1:2 cm$^3$; each 3 cm$^3$ of diluted sample or standard was mixed with 0.5 cm$^3$ of 10:1 formaldoximine/$NH_4OH$ reagent; color read in a 1-cm cell at 450 nm. |

**Appendix A. (Continued)**

| | | | | | |
|---|---|---|---|---|---|
| 7. | $NO_3^-$ & $NO_2^-$ | spectrophotometry/ Cd-reduced samples | ±10% | Gieskes and Peretsman (1986) | 1 $cm^3$ volumes of acidified samples and standards (0-50 µM $NO_3^-$) were mixed with 9 $cm^3$ of double-distilled water and neutralized with 0.5N $NaHCO_3$ soultion; each diluted sample was mixed with 100λ concentrated $NH_4Cl$ and run through a pre-conditioned Cd-wire column; 3$cm^3$ of the reduced solution was combined with 100λ sulfanilamide reagent; within 2-8 minutes, 100λ N-1-naphthyl-ethylene diamine solution was added and mixed; color read within 0.25-2 hours in a 1-cm cell at 543 nm. |
| 8a | $\Sigma H_2S$ | spectrophotometry | ±3% | Cline (1969) | Under a $N_2$ atmosphere and immediately after filtering, 0.25-1.0 $cm^3$ of sample or standard (0-1000 µM $\Sigma H_2S$) was pipetted into a vial containing 0.1$cm^3$ of mixed diamine reagent (Cline's B or D reagent); if necessary the volume was brought up to 1.1 $cm^3$ with double distilled water; after 20 minutes all samples and standards that were reacted with D reagent were diluted by mixing 0.1 $cm^3$ in 5 $cm^3$ of double-distilled water; color of all B, diluted D samples and standards read in a 1-cm cell at 670 nm. |
| 8b | $\Sigma H_2S$ | monobromobimane-HPLC | ±1% | Vetter et al. (1989) | Under a $N_2$ atmosphere, 0.1 $cm^3$ pore water aliquots were pipetted directly from the centrifuge tubes before filtering; these were reacted with 10λ monobromobimane solution; proteins were precipitated by adding 100 λ acetronitrile and heating at 60°C; samples were then mixed with 290λ methane sulfonic acid, centrifuged and frozen; in the laboratory, the derivatized samples were separated by HPLC on a C-18 reverse-phase column with a methanol-water gradient and quantified by fluorecence. |
| 9a | $SO_4^{2-}$ | turbidometry | ±1 mM | Tabatabai (1974) | 0.1 $cm^3$ of unacidified sample or standard (0-28 mM $SO_4^{2-}$) was mixed with 3 $cm^3$ double-distilled water and 0.1 $cm^3$ 1N HCl; 0.1 $cm^3$ Difco Gelatin/$BaCl_2$ reagent was added and the mixture was homogenized; after exactly 30 minutes, turbidities were read in a 1-cm cell at 420 nm. |
| 9b | $SO_4^{2-}$ | anion chromatography | ±0.1 mM | Gieskes and Peretsman (1986) | Unacidified samples and IAPSO standard seawater (28.9 mM $SO_4^{2-}$) were diluted 1000-fold with double-distilled water; volumes of 0.3-0.5 $cm^3$ were injected into the 0.05 $cm^3$ ion chromatograph sample loop, and peak heights recorded on a strip chart recorder. |
| 10 | $Ca^{2+}$ | EGTA titration | ±0.04 mM | Gieskes and Peretsman (1986) | 0.5 $cm^3$ of sample was mixed with 3 $cm^3$ distilled water; while stirring 0.5 $cm^3$ of GHA reagent and 0.5 $cm^3$ of borate buffer were added; each mixed was titrated with 10 mM EGTA solution to an end point indicated by a change from red to colorless; IAPSO seawater (10.55 mM $Ca^{2+}$) was used for standardization. |
| 11 | $Mg^{2+}$ | EDTA titration | ±0.1 mM | Gieskes and Peretsman (1986) | Total alkaline earths, i.e., $Ca^{2+}$, $Mg^{2+}$ and $Sr^{2+}$, were determined and $Mg^{2+}$ calculated using the $Ca^{2+}$ titration value. 0.5 $cm^3$ of sample was mixed with 5 $cm^3$ double-distilled water, 1 $cm^3$ ammonia buffer, and 0.1 $cm^3$ indicator solution; while stirring, each mixture was titrated with 0.03 M EDTA solution to an end point indicated by a color change from red to blue; IAPSO seawater (total alkaline earths 64.54 mM) was used for standardization. |
| 12 | Total Alkalinity | potentiometric titration | ±0.05 mM | Gieskes and Peretsman (1986) | 1 $cm^3$ of unacidified sample was transfered to a 5 $cm^3$ polystyrene tube held in a temperature controlled water jacket. A combination pH electrode was inserted into the sample and the EMF recorded after ten incremental additions (0.002 $cm^3$) of 0.1 N HCl; the acid was standardized against a solution of 0.1 M sodium borate and 0.55 M sodium chloride. |

*Precision based on 2 times the standard deviation of duplicate or triplicate analyses of random samples.
BC = box core, K= Kasten core, 1λ = $10^{-3}$ $cm^3$, Σ indicates total species